PHYSICAL REVIEW D **93,** 014028 (2016)

Reassessing the discovery potential of the $B \to K^* \ell^+ \ell^-$ decays in the large-recoil region: SM challenges and BSM opportunities

S. Jäger[1] and J. Martin Camalich[2,3]

[1]*Department of Physics and Astronomy, University of Sussex; Brighton BN1 9QH, United Kingdom*
[2]*Department of Physics, University of California, San Diego, 9500 Gilman Drive, La Jolla, California 92093-0319, USA*
[3]*PRISMA Cluster of Excellence Institut für Kernphysik, Johannes Gutenberg-Universität Mainz, 55128 Mainz, Germany*

(Received 6 March 2015; published 27 January 2016)

We critically examine the potential to disentangle the Standard Model (SM) and new physics (NP) in $B \to K^* \mu^+ \mu^-$ and $B \to K^* e^+ e^-$ decays, focusing on (i) the LHCb anomaly, (ii) the search for right-handed currents, and (iii) lepton-universality violation. Restricting ourselves to the large-recoil region, we advocate a parametrization of the hadronic matrix elements that separates model-independent information about nonperturbative QCD from the results of model calculations. We clarify how to estimate corrections to the heavy-quark limit that would generate a right-handed (virtual) photon in the $b \to s\gamma$ contribution to the decay. We then apply this approach to the discussion of various sets of observables of increasing theoretical cleanness. First, we show that angular observables in the optimized $P_i^{(\prime)}$ basis are, in general, still not robust against the long-distance QCD effects, both numerically and by examining analytically the dependence on corrections to the (model-independent) heavy-quark limit. As a result, while a fit to data favors a NP contribution to the semileptonic operators of the type $\delta C_9 \simeq -1.5$, this comes at a relatively small statistical significance of $\lesssim 2\sigma$ once such power corrections are properly accounted for. Second, two of these observables, P_1 and P_3^{CP}, are particularly clean at very low q^2 and sensitive probes of right-handed quark currents. We discuss their potential to set stringent bounds on the Wilson coefficient C_7', especially using data of the electronic mode, and we update the bounds with current angular data in the muonic channel. Finally, in light of the recent hint of lepton-universality violation in $B^+ \to K^+ \ell\ell$, we introduce and investigate new lepton-universality observables involving angular observables of the muonic and electronic modes and their zero crossings and show that, if the effect is of the size suggested by experiment, these can clearly distinguish between different NP explanations in terms of underlying semileptonic operators.

DOI: 10.1103/PhysRevD.93.014028

I. INTRODUCTION

Rare B decays such as $B \to M \ell^+ \ell^-$, where M is a charmless hadronic state, are powerful probes of beyond Standard Model (BSM) physics due to their short-distance sensitivity combined with their GIM and CKM suppression in the Standard Model (SM). In case M is a vector resonance, like the $K^*(892)$ (K^* from now on), the decays have a very rich kinematical structure that leads to up to 24 angular observables (including direct CP asymmetries) which are functions of the dilepton invariant mass squared, q^2 [1–38].

Experimental results on $B \to K^* \ell^+ \ell^-$ include measurements of the branching fraction, forward-backward asymmetry and the longitudinal polarization fractions by the B-factories [39–42], CDF [43], LHCb [44,45], CMS [46] and ATLAS [47]; measurements including the angular observables $A_T^{(2)}$ and $A_{\rm im}$ have been done by CDF [48] and LHCb [45]. Intriguingly, LHCb reported a 3.7σ discrepancy with the SM in the muonic mode ($\ell = \mu$) in the course of the first complete (CP-averaged) angular analysis of the final state system [49]. The putative effect occurs in the $[4.3, 8.68]\ \mathrm{GeV}^2$ dilepton mass bin of the angular observable P_5', but also with a lower significance of 2.5σ in the bin $[1, 6]\ \mathrm{GeV}^2$. Other tensions have been pointed out in the data (P_2 [50] or F_L [51]) and global analyses of $b \to s\mu\mu$ and $b \to s\gamma$ decays have claimed the data to be in tension with the SM with a statistical significance of up to 4.5σ [50].

Beyond the SM, this tension can be ascribed to a negative shift of the Wilson coefficient of the semileptonic-vector operator Q_9 [50] in the weak Hamiltonian, although contributions to other Wilson coefficients have also been discussed [50–54]. On the other hand, a previous analysis of the angular observables using a model-independent parametrization of the hadronic uncertainties [33] that minimized the input from nonperturbative calculations, led to SM predictions with theoretical errors considerably larger than those employed in the above-mentioned fits. More recently, a Bayesian analysis of the data found a good agreement with the SM [52], allowing the hadronic parameters to float in the fit.

Besides that, the LHCb recently reported an even more surprising deficit of $B^+ \to K^+\mu\mu$ decays as compared to $B^+ \to K^+ ee$, with a significance of 2.6σ [55]. This signal of lepton-universality violation (LUV) has been analyzed by different groups [56–62] with the common conclusion that the only plausible sources of this effect are the semileptonic operators $Q^{(\prime)}_{9,10}$. Moreover, it was recently pointed out [62] that similar deficits in the inclusive $b \to s\ell\ell$ decay have been observed by Belle [63] and *BABAR* [64].

Because of the far-reaching implications of potential manifestations of new-physics (NP), a clear understanding of the SM "background" expectation is needed. In this work, we critically re-examine the anatomy of the uncertainties in the theoretical description of $B \to K^*\ell^+\ell^-$ decays in the large-recoil region and classify different observables according to their theoretical cleanness. Our presentation draws on our longer work [33], which was focused on a transparent decomposition of the decay amplitudes into (perturbatively) calculable and nonperturbative ingredients, a general but minimal parametrization of the latter, and a discussion of present and prospective knowledge of those parameters. The framework in [33] was tailored to the lower end-point region of the dilepton invariant mass spectrum. We update it here and, with minor extensions, we apply to the case at hand.

We then update our SM predictions for the angular distribution of $B \to K^*\mu^+\mu^-$ and provide new predictions for the $B \to K^* e^+ e^-$ angular distribution. The complex dependence that observables in the $P^{(\prime)}_i$ basis, in general, have on the underlying hadronic matrix elements is illustrated analysing the tension of the $b \to s\mu\mu$ data with the SM. We further discuss two observables, P_1 and P_3^{CP}, which are particularly clean and that can be used to put stringent bounds on electromagnetic operators induced by right-handed currents. Finally, in light of the LUV signals hinted by different $b \to s\ell\ell$ measurements we introduce and study new lepton-universality ratios which are very accurately predicted in the SM. We show that they provide an excellent benchmark to confirm and characterize the effect and we study prospects in different NP scenarios.

II. CONNECTING SHORT-DISTANCE PHYSICS TO OBSERVABLES

The decay $\bar{B} \to \bar{K}^*\ell^+\ell^-$ proceeds via the $\Delta B = 1$ weak Hamiltonian (see e.g. [65]), which encapsulates short-distance SM contributions from scales above $\mu \sim m_b$, as well as any NP with mass scale beyond the weak scale, in a set of Wilson coefficients. In the SM, the lepton pair is always produced through either the leptonic vector or axial vector current. The three axial vector helicity amplitudes are

$$H_A(\lambda) = -iN\tilde{V}_\lambda(q^2)C_{10}, \tag{1}$$

where λ is the helicity of the $\bar{K}^*$ and N a normalization constant. They receive contributions only from the semileptonic part of the weak Hamiltonian and factorize "naively" into helicity form factors $\tilde{V}_\lambda(q^2)$ ([33,66]; conventions in this paper follow [33]) and the Wilson coefficient C_{10}.

If the lepton mass is not neglected, the axial-vector current can also create the dilepton in a pseudoscalar state ($\lambda = 0$ only), bringing in another, naively factorizing, amplitude $H_P(q^2) = -iN\frac{2m_\ell|\vec{k}|}{q^2}\frac{m_b}{m_b+m_s}S(q^2)C_{10}$, (equivalent to what is often called "timelike" amplitude), and one extra, scalar form factor S; $|\vec{k}| = \lambda^{1/2}(m_B^2, m_{K^*}^2, q^2)/(2m_B)$ is the momentum of the vector meson in the B-meson rest frame.

In addition, the dilepton can be produced through the vector leptonic current. The corresponding three vector helicity amplitudes $H_V(\lambda)$ again receive contributions from the semileptonic $\Delta B = 1$ Hamiltonian. However, they comprise further terms originating in the magnetic penguin operator $Q_{7\gamma}$, as well as from the hadronic part of the weak Hamiltonian, whereby the dilepton is created through a virtual photon. The former bring in a further set of three form factors, while the latter contributions include "charm loops," "annihilation," etc. and do not factorize naively. In the notation of [33]:

$$H_V(\lambda) = -iN\left[\tilde{V}_\lambda(q^2)C_9 + \frac{2m_b m_B}{q^2}\tilde{T}_\lambda(q^2)C_7 - \frac{16\pi^2 m_B^2}{q^2}h_\lambda(q^2)\right]. \tag{2}$$

Beyond the SM, the helicity amplitudes may receive extra contributions from modified Wilson coefficients C_7, C_9, C_{10}, as well as the chirality-flipped operators, Q'_7, Q'_9, Q'_{10}, if present. Furthermore, in the most general NP scenario there will a be further "scalar" and three "tensor" amplitudes.[1]

We would like to emphasize the simplicity and transparency of (1) and (2) when compared to the more traditional transversity amplitudes involving chiral lepton currents. In particular, it exposes in a clear way the various hadronic uncertainties impacting on the vector helicity amplitudes, which stem from two rather than one form factors (per helicity), $\tilde{V}_\lambda$ and $\tilde{T}_\lambda$, and, in addition, the nonlocal correlator h_λ. While the photon-pole dominance can be exploited to identify especially clean null tests of the SM at very low q^2, particular care will be needed in attributing BSM effects to observables that involve the vector helicity amplitudes (e.g. through C_9) away from the end point of the large-recoil region.

[1]The NP scalar contributions to $B \to K^*\ell^+\ell^-$ are tightly bounded by the pure leptonic rare decay $B_s \to \ell^+\ell^-$ [14,56]. Tensor operators can be neglected if we assume the scale of NP to be well above the electroweak scale [56].

Finally it is worth recalling that the residues of the vector helicity amplitudes are related to the amplitude of the radiative decay:

$$\mathcal{A}(\bar{B}\to K^*(\lambda)\gamma(\lambda)) = \lim_{q^2\to 0}\frac{q^2}{e}H_V(q^2=0;\lambda) = \frac{iNm_B^2}{e}\left[\frac{2m_b}{m_B}(C_7\tilde{T}_\lambda(0) - C_7'\tilde{T}_{-\lambda}(0)) - 16\pi^2 h_\lambda(q^2=0)\right]. \quad (3)$$

A. Minimal parametrization of nonperturbative QCD

The key to understanding the uncertainties on various observables is a full and transparent description of the nonperturbative input, both of the factorizable (form factor) and (naively) nonfactorizable (h_λ) type. This allows to disentangle model-independent constraints from assumptions in the modeling of nonperturbative QCD effects.

A considerable simplification of the nonperturbative dynamics arises in the combined heavy-quark and large-energy (HQ/LE) limit of QCD [67–73], corresponding to the large-recoil or low-q^2 region of the decay. In this limit, both the form factors [68,74,75] and the (naively) nonfactorizable term h_λ [5,9] exhibit QCD factorization (collinear factorization) into universal "soft" form factors, light-cone distribution amplitudes (LCDA), and perturbatively calculable hard kernels; this structure is most transparent when formulated in soft-collinear effective field theory (SCET) where the hard kernels become Wilson coefficients of operators built out of collinear and soft fields [71–73]. In particular, the number of independent form factors is reduced from seven to two, the vector and tensor helicity form factors in (2) are related, and two helicity amplitudes vanish altogether.

A fundamental limitation to factorization is the fact that $\mathcal{O}(\Lambda/E, \Lambda/m_B)$ power corrections (to be denoted generically by $\mathcal{O}(\Lambda/m_B)$ from now on), do not factorize; attempts to do so lead to end-point divergent convolutions. Therefore, besides the parametric uncertainties entering the amplitude in the exact HQ/LE limit, one needs to take into account these power corrections. In this section we update and extend the model-independent treatment of power corrections introduced for the first time in [33]. We stress at the outset that this issue cannot be sidestepped by employing form factor calculations in the light-cone sum rule (LCSR) framework (or other existing frameworks). To the extent that LCSR calculations give an unambiguous, controlled (i.e. systematically improvable) approximation, they involve convolutions of perturbative kernels with LCDA and a twist expansion very similar, and underpinned by very similar Feynman diagram calculations, as those applying to the heavy-quark expansion. However, these are necessarily accompanied by model-dependent steps before a hadronic quantity can be extracted, most importantly a modeling of an infinite tower of continuum contributions. While there is a standard convention for attaching uncertainties due to this, the procedure is quantitatively justified only by a number of numerical successes. We will, however, clarify in what sense LCSR calculations can be used to estimate *corrections* to the HQ/LE limit, for which much less relative accuracy is required. This was shown in detail for the helicity +1 form factors in [33]. Below we will also clarify further in what sense the leading corrections to the heavy-quark limit of h_+ can be precisely identified with a matrix element that can be estimated with the LCSR method as done in [33].

1. Form factors

We start rescaling the helicity-zero form factors:

$$V_0(q^2) = \frac{\sqrt{q^2}}{|\vec{k}|}\tilde{V}_0(q^2), \qquad T_0(q^2) = \frac{m_B^2}{\sqrt{q^2}|\vec{k}|}\tilde{T}_0(q^2),$$
$$V_\pm(q^2) = \tilde{V}_\pm(q^2), \qquad T_\pm(q^2) = \tilde{T}_\pm(q^2). \quad (4)$$

In [33], a parametrization of the following form was suggested:

$$F(q^2) = F^\infty(q^2) + a_F + b_F q^2/m_B^2 + \mathcal{O}([q^2/m_B^2]^2). \quad (5)$$

Here F denotes any helicity form factor with $F^\infty(q^2)$ its HQ/LE limit, and the remainder the power corrections. More precisely, $F^\infty(q^2)$ are functions (one for each form factor) among which the HQ/LE relations hold, including perturbative corrections [68,74,76]. The precise form of $F^\infty(q^2)$ is ambiguous (see below) and defines a scheme for the power correction terms.

In (5), we have Taylor-expanded the power corrections about $q^2 = 0$. As the form factors have no singularity in a circle of radius $m_{B_s}^2$ about the origin in the complex q^2 plane, this amounts to an expansion in the dimensionless ratio $q^2/m_{B_s}^2$ with coefficients of generic size $\mathcal{O}(\Lambda/m_B)$. In particular, the remainder term in (5) should be a correction of a few percent throughout the low-q^2 region $q^2 < 6\ \mathrm{GeV}^2$, and will be neglected in the following (see also [38]). We stress that beyond this truncation there is no loss of generality in our decomposition.

The form factors obey a number of model-independent relations. First, there are two exact constraints:

$$T_+(0) = 0, \qquad S(0) = V_0(0). \quad (6)$$

Five further constraints hold in the HQ/LE limit, two to all orders[2] in α_s:

[2]This was conjectured in [77], exhibited at $\mathcal{O}(\alpha_s)$ in [33] and follows at $\mathcal{O}(\alpha_s^2)$ from the results of [76]. It seems nevertheless clear that it is true to all orders [75].

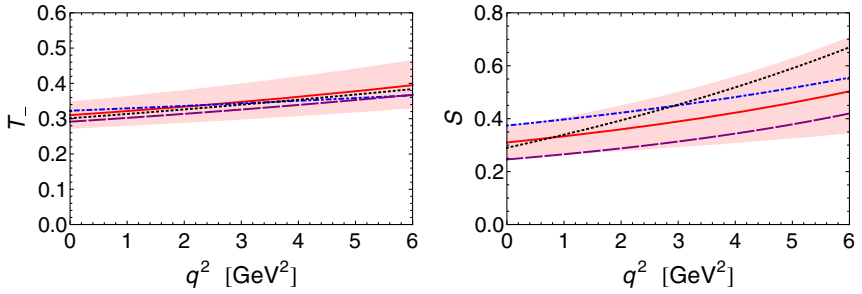

FIG. 1. The QCD form factors employed in this work to determine the soft form factors, $T_-(q^2)$ and $S(q^2)$ (red solid), compared to the determinations used as input in the LCSRs [78] (blue short-dashed), [79] (black dotted) and Dyson-Schwinger equations [80] (purple long-dashed) approaches. Note that the error of $T_-(0)$ has been enlarged to cover the experimentally driven determinations (see text).

$$V_+^\infty(q^2) = 0, \qquad T_+^\infty(q^2) = 0, \tag{7}$$

and three to zeroth order in perturbation theory only:

$$V_-^\infty(q^2) = T_-^\infty(q^2), \qquad V_0^\infty(q^2) = T_0^\infty(q^2),$$
$$V_0^\infty(q^2) = S^\infty(q^2). \tag{8}$$

The perturbative corrections to (8) are unambiguously calculable as convolutions of perturbative kernels with nonperturbative LCDA [74]. Eqs. (7) and (8) reduce the nonperturbative input in the exact HQ/LE limit from seven to two independent functions; i.e., there are only two independent $F^\infty(q^2)$, traditionally called the "soft form factors." From (8) it is clear that they correspond to the helicities -1 and 0, denoted $\xi_\perp(q^2)$ and $\xi_\parallel(q^2)$, respectively. Their q^2 dependence is not calculable from first principles at present (the scaling in [68] is violated by radiative corrections [74]); as a result, not only the values at $q^2 = 0$ of the soft form factors but also their q^2 dependence need to be modeled or determined experimentally.

At finite m_B, where the power corrections are nonzero, the soft form factors are not uniquely determined, as the HQ/LE relations are invariant under a shift,

$$\xi_\perp(q^2) \to \xi_\perp(q^2) + f_\perp(q^2),$$
$$\xi_\parallel(q^2) \to \xi_\parallel(q^2) + f_\parallel(q^2), \tag{9}$$

where $f_\perp$ and $f_\parallel$ are $\mathcal{O}(\Lambda/m_B)$. It is customary to exploit this freedom by identifying $\xi_\perp(q^2)$ and $\xi_\parallel(q^2)$ with a pair of (finite-m_B) QCD form factors.

In this work we use

$$\xi_\perp(q^2) = T_1(q^2) = \frac{m_B}{2|\vec{k}|} T_-(q^2) - b_{T_+} \frac{q^2}{2m_B|\vec{k}|} + \mathcal{O}\left(\frac{\Lambda^2}{m_B^2}; \frac{\Lambda}{m_B}\left(\frac{q^2}{m_B^2}\right)^2\right),$$
$$\xi_\parallel(q^2) \equiv S(q^2), \tag{10}$$

where $T_1(0)$ is a tensor form factor in the transversity basis. We parametrize the q^2 dependence by modifying the HQ/LE scalings of [68]:

$$\xi_X(q^2) = \xi_X(0)\left(\frac{1}{1 - q^2/m_B^2}\right)^{2+\alpha_X}, \qquad X = \perp, \parallel. \tag{11}$$

The values at $q^2 = 0$,

$$\xi_\perp(0) = T_-(0) = 0.31(4), \qquad \xi_\parallel(0) = 0.31(6), \tag{12}$$

are obtained as an average of results based on LCSR [78,79] and Dyson-Schwinger equations [80]; hereby, the errors are chosen such that the central values of these predictions are covered, as is the value of $T_-(0)$ suggested by the observed $B \to K^*\gamma$ branching fraction, $T_-(0) \simeq T_1(0) = 0.277(13)$ [5,14,33].[3] We note that the identification $\xi_\perp(0) = T_-(0)$ implicitly fixes a nonvanishing value of the $\mathcal{O}(\Lambda^2/m_B^2)$ residual term in (10). The parameters α_X in (11) model the nonperturbative radiative violations to the "naive" HQ/LE scaling; we estimate them comparing again to the different calculations:

$$|\alpha_\perp|^{\max} = 0.2, \qquad |\alpha_\parallel|^{\max} = 0.7. \tag{13}$$

In Fig. 1 we show the $T_-(q^2)$ and $S(q^2)$ used in this work compared to the central values of the calculations used as input. The error bands stem from the parameters $\xi_X(0)$ and α_X, that, together with the parameters in the α_s corrections [74] to Eqs. (8) (see below), represent the only sources of theoretical uncertainties that enter the helicity amplitudes through the form factors in the HQ/LE limit.

While our errors on the soft form factors may seem to dwarf the power corrections, this is a mirage: experimentally, one studies observables for which the dependence on the soft form factors cancels out if α_s and power corrections are neglected. Hence, the latter, parametrized by the

[3]The latter assumes that there is no NP in C_7 or C_7'. The former Wilson coefficient is strongly constrained by inclusive $B \to X_s\gamma$ decay, and we assume it to be given by its SM value in this paper. The latter is constrained independently to be (in the present context) negligibly small by other observables as discussed and quantified in Sec. III D.

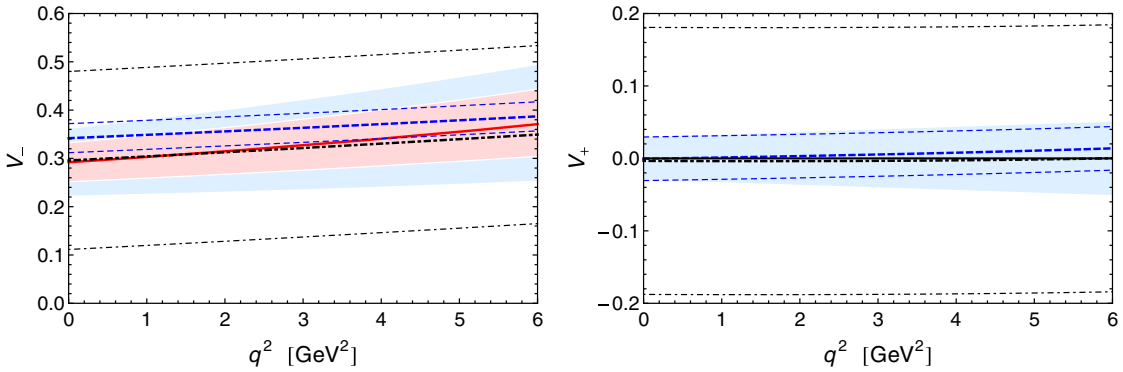

FIG. 2. The predictions on the form factors $V_-(q^2)$ and $V_+(q^2)$ obtained in the QCDF approach described in this work. The blue band are the uncertainties from power corrections added linearly to those from the errors of the parameters entering the perturbative corrections (red band). These are compared to results in two different LCSR calculations, [78] (blue dashed) and [79] (black dot-dashed), where the thinner lines are the errors obtained ignoring correlations and taking the maximum possible value when transforming to the helicity basis used here.

coefficients a_F and b_F in (5), constitute a leading source of uncertainty on these observables and must be carefully considered. First, the exact relations (6) imply

$$a_{T_+} = 0, \qquad a_{V_0} = a_S. \tag{14}$$

On the other hand, the pairs of coefficients $a_{T_-} = a_S = 0$ and $b_{T_-} = b_S = 0$ since they are effectively absorbed in $\xi_{\perp,\parallel}(0)$ and $\alpha_{\perp,\parallel}$, respectively, through the definitions of the soft form factors detailed above. This, in turn, also implies that $a_{V_0} = 0$ using the second equation in (14). Note that we cannot remove the remaining eight coefficients a_{T_0}, b_{T_0}, a_{V_-}, b_{V_-}, a_{V_+}, b_{V_+}, b_{T_+} and b_{V_0} while maintaining the heavy-quark relations (8).

These are dimensionless coefficients which represent a suppression $\mathcal{O}(\Lambda/m_B)$ over the values (for a_F) and first derivatives (for b_F) of the form factors at $q^2 = 0$. From the results in the HQ/LE limit we see that $F(0) \sim \xi_X(0) \simeq 0.3$, while for the slopes Eq. (11) leads to $dF(q^2)/dq^2|_{q^2=0} = \xi_X(0)(2+\alpha_X)/m_B^2$, which, taking into account Eq. (13), can be numerically as large as ~ 1 (in units of m_B^{-2}). Thus, assuming for the moment that $\Lambda/m_B \sim 0.10$, we find from power-counting arguments alone that

$$|a_F^{\mathrm{max,pc}}| \simeq 0.03, \qquad |b_F^{\mathrm{max,pc}}| \simeq 0.10. \tag{15}$$

One should keep in mind that these estimates are *ad hoc* when interpreting the uncertainties derived from the bounds in (15). To be more precise, and except for their generic Λ/m_B suppression we assume that the exact size (and sign) of the power corrections are currently unknown.

One can also use the model-independent parametrization in Eq. (5) to implement further constraints that could be obtained from first-principles in QCD or to build in nonperturbative calculations of the form factors and test them (see e.g. [38]). This discussion is of the utmost importance in instances where experimental tensions with the SM appear in observables that are not only sensitive to short-distance Wilson coefficients but also to the power corrections to the form factors.

In connection to this, and as an illustration that will become useful for the phenomenological discussion below, we show in Fig. 2 the vector form factors $V_\pm(q^2)$ used in this work together with two different predictions from LCSRs. It is interesting to note at this point that the calculation in [78] implies a power correction to $V_-(q^2)$ which is consistent with the power-counting estimate in (15) but favoring an overall *positive* sign, i.e.

$$\frac{V_-(0)}{T_-(0)} \gtrsim \frac{V_-^\infty(0)}{T_-^\infty(0)}. \tag{16}$$

Finally, let us also remark that the identifications used in Eq. (12) are arbitrary and other QCD form factors could have been employed in their stead. This amounts to re-arrangements of power corrections, cf. Eq (9), so that comparing different schemes allows to test the robustness of the approach introduced in [33] and refined here. Our particular choice is different to the one taken in [29,31] which is based on using the vector form factors, i.e. $V_-(q^2)$ and $V_0(q^2)$ in the helicity basis. We prefer to retain the tensor form factor $T_-(q^2)$ because its value at $q^2 = 0$ can be determined from experimental data [33,74]. The form factor $S(q^2)$ appears in the amplitude only multiplied by lepton masses, and it is argued in Ref. [38] that using $V_0(q^2)$ to fix $\xi_\parallel(q^2)$ in its stead could reduce the impact of the power corrections in the predictions. However, Eq. (14) implies that the power corrections to $V_0(q^2)$ enter only through b_{V_0} which has a marginal effect in the total uncertainty. We will explicitly demonstrate this by comparing both choices in the phenomenological discussion below.

2. Nonfactorizable term

The matrix element of the hadronic weak Hamiltonian, affecting only the three vector helicity amplitudes through

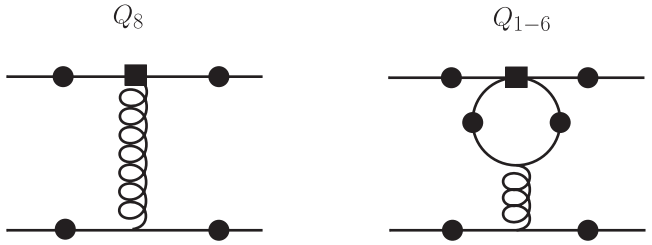

FIG. 3. Spectator scattering diagrams for $B \to V\gamma^{(*)}$. The bullets denote the possible photon attachments.

the h_λ terms in (2), can also be split into a HQ/LE limit and a power correction term,

$$h_\lambda(q^2) = h_\lambda^\infty(q^2) + r_\lambda(q^2). \tag{17}$$

The leading-power term h_λ^∞ can be calculated systematically to any order in α_s in QCD factorization [5]. It carries a well-defined q^2 dependence. In particular, to $\mathcal{O}(\alpha_s^0)$ it amounts to the well-known substitutions $C_7 \to C_7^{\rm eff}$ and $C_9 \to C_9^{\rm eff}(q^2)$ in (2) and the addition of a single, CKM-suppressed annihilation diagram.

The power-correction terms r_λ are more complicated than in the form factor case. The hadronic weak hamiltonian comprises two operators Q_1^c, Q_2^c involving a charm quark pair, as well as four-quark operators containing light quarks and the chromomagnetic penguin operator. Of these, the charmed operators come with large CKM and Wilson coefficients, presumably giving the most important contributions that we will denote by r_λ^c.

A key conclusion in [33] was that while r_λ^c is *not* negligible for $\lambda = -, 0$, it respects the same helicity hierarchy as the factorizable terms, i.e. $|r_+^c| \ll |r_-^c|, |r_0^c|$. This relied on a LCSR estimate of soft gluon emission from the charm loop, and we clarify here the precise relation to the QCD factorization result in the heavy-quark limit.

Recall first that the HQ/LE limit is given in terms of Feynman diagrams such as those shown in Fig. 3, computed for soft "constituents" of the B-meson and collinear ones of the K^*, convoluted with leading-twist light-cone distribution amplitudes. Schematically,

$$h_\lambda = \int_0^1 du \phi_{K^*}(u) T(u, \alpha_s) + \mathcal{O}(\Lambda/m_b), \tag{18}$$

where u is the fraction of the K^* momentum carried by one of the K^* constituents and dependence on the B-meson constituent momenta has been suppressed. The internal lines in the graphs can have hard $[\mathcal{O}(m_b^2)]$ or hard-collinear $[\mathcal{O}(m_b\Lambda)]$ virtualities. A Wilsonian picture is provided (just as for the form factor case) by SCET, whereby in two matching steps the hard and the hard-collinear degrees of freedom are integrated out, leaving a theory with only $\mathcal{O}(\Lambda^2)$ virtualities, where soft and collinear modes no longer talk to each other and $T(u, \alpha_s)$ is a Wilson coefficient. In fact the picture is not quite complete, as some convolutions are not convergent: these, however, can be absorbed into heavy-to-light form factors, times so-called vertex corrections. There are also annihilation graphs that converge for $\lambda = \pm 1$ for all q^2. A necessary and sufficient requirement for convergence is a sufficiently fast fall-off of the LCDA at the end point, which holds at leading twist. This ensures that the "end-point" contributions to the convolutions, where the collinear "constituent" really is soft, and the LCDA formalism does not apply, is suppressed by at least one power of Λ/m_B [70].

Further sources of power corrections arise from similar graphs (with two K^* "constituents") convoluted with higher-twist two-particle LCDAs, and from graphs with more constituent lines convoluted with multi-particle LCDAs (also of higher twist). Sometimes, such higher-twist contributions exhibit end-point divergences. Note that at the (spectator) end point, the virtualities of the internal lines are reduced. For example, the gluon in Fig. 3 is generically hard-collinear, but soft in the endpoint region, if the photon does not attach to the spectator line. One can introduce a cutoff Λ_h separating collinear from soft momenta. Then schematically,

$$r_\lambda^c \sim \int_{\Lambda_h}^1 du \phi_{K^*}(u) T(u, \alpha_s) + r_{\lambda,\rm soft}^c. \tag{19}$$

The first term represents the contributions involving hard-collinear gluon exchanges and is calculable in perturbation theory (albeit cutoff dependent). The second contribution cannot be computed in QCD factorization, however it can be represented by an operator matrix element $\langle K^*|O_{\bar{s}Gb}|B\rangle$ where $O_{\bar{s}Gb}$ is an operator involving one soft gluon field. The end-point contribution in this case would not have a relative power suppression; this can again be argued based on the end-point behavior of the LCDA and kernel [70], or simply on the grounds that, even though not calculable, it needs to cancel the cutoff dependence.

At the two-particle LCDA level, the hard-collinear term for an insertion of the $(V-A)\times(V-A)$ operators Q_1^c, Q_2^c cannot generate an r_+^c amplitude because of chirality conservation in QCD (if light-quark masses are neglected) [74,77]. It is clear that this also applies to the twist-3 (first subleading power) two-particle contribution. There are also twist-3 three-particle contributions, corresponding to an extra outgoing collinear gluon line. They do not vanish by the $V-A$ structure of weak interaction, as the extra gluon field can carry helicity $+1$. These three-particle twist-3 contributions have not been computed in the literature.[4] In LCSR computations of the $B \to V$ form factors, they give small contributions [81]. For the present case, we note that

[4]A subset of twist-3 two-particle contributions relevant to the isospin asymmetries in $B \to K^*\gamma$ and $B \to K^* l^+ l^-$ has been calculated in [7,8].

the hard-collinear contributions are suppressed by a factor of α_s, and it appears clear that they are end-point convergent from the fact that the three-particle twist-3 vector meson LCDA vanishes linearly at the quark and antiquark end points (and quadratically at the gluon end point) [82].

In summary, all hard-collinear contributions are at least Λ^2/m_B^2 or $\Lambda/m_B \times \alpha_s$ suppressed, and the same is true for any contribution involving a collinear gluon, including if extra soft gluons are radiated. Hence the fate of r_+^c is determined (at order Λ/m_B) by purely soft gluon emission from the charm loop, while r_-^c, r_0^c receive small corrections to their nonvanishing leading-power values from this mechanism. For $q^2 \ll 4m_c^2$, the interaction of the charm loop with a soft gluon background can be represented through a series of light-cone operators with matrix elements scaling as $[\Lambda^2/(4m_c^2)]^n$, $n = 1, 2, \ldots$ [79].[5] The $B \to K^*$ matrix element of the leading (1-soft-gluon) term in this operator expansion provides an approximation of $r_{\lambda,\text{soft}}^c$, accurate up to $\Lambda^4/(4m_c)^4)$ corrections. We have verified that the result in [79] corresponds to the identification $\Lambda m_B \sim 4m_c^2$. One obtains generic sizes of Λ/m_B for $r_{\lambda,\text{soft}}^c$, as expected. For $q^2 = 0$ this was indeed the conclusion reached already in [83].

To go further in estimating the hadronic matrix elements, in [33] we adapted a LCSR developed in [79] to the helicity amplitudes r_λ^c. LCSRs equate the matrix element of a perturbative two-point correlator to a sum over a complete set of hadronic states, which is then truncated to its first term by means of a duality threshold model. This first term contains the desired hadronic matrix element. In the case at hand, the correlation function vanishes for $\lambda = +1$ up to terms suppressed by an extra factor of Λ/m_B [33]. Barring systematic cancellations between the different terms in the hadronic sum, for which we cannot identify a mechanism, this implies that $r_+^c = \mathcal{O}(\Lambda^2/m_B^2)$. No such suppression takes place for $\lambda = -, 0$, which are $\mathcal{O}(\Lambda/m_B)$.

Based on these considerations, we parametrize the remainder term as:

$$r_\lambda^c(q^2) = A_\lambda + B_\lambda \frac{q^2}{4m_c^2}, \tag{20}$$

where A_λ and B_λ are constants of order $\Lambda^2/(4m_c^2)$. This generalizes the parametrization in [33], where $r_\lambda(q^2)$ was approximated by its $q^2 = 0$ value, equivalent to a shift in the Wilson coefficient C_7 in (2) and appropriate for the phenomenological discussion for $q^2 \leq 3$ GeV^2, a restriction we do not wish to make here. The B_λ-terms parametrize the leading corrections to a pure $1/q^2$ dependence once the photon propagator is taken into account, and give rise to a q^2-independent contribution to the amplitude, and an estimate of the uncertainty due to long-distance charm contributions away from the kinematic end point. Attempts to improve on this by including higher powers of $q^2/(4m_c^2)$ appear futile, as those will only become relevant once $q^2/(4m_c^2) \sim 1$ and the expansion breaks down.

Concerning the numerical values of A_λ and B_λ, we allow arbitrary complex phases for them. This is because, even when restricting to the operators Q_1^c and Q_2^c, r_λ is affected by "charmless" multiparticle cuts, just as happens already in the leading-power, perturbatively calculable charm loop result [5]. (See also the discussion in terms of hadronic final state interactions in [84].) Although this means that the q^2 dependence is not analytic in any disc around the origin, the dependence on the charm mass should still be regular and admit an expansion in the variable $q^2/(4m_c^2)$ (with m_c-independent, nonanalytic coefficients), as the charm quark pair is always off shell. In practice allowing an arbitrary strong phase has little effect on the uncertainties on the observables considered below.

It is instructive to represent r_λ^c as a (helicity-dependent) shift to $C_9^{\text{eff}}(q^2)$. In Fig. 4 we show the long-distance charm contributions used in this work parametrized as a correction to the Wilson coefficient C_9. The (black) solid line is the result of a fit of Eq. (20) to the upper error band shown in Fig. 5 of Ref. [79] that is the result of the LCSR calculation valid up to $q^2 \simeq 4$ GeV^2. We show the modulus of the (complex) correction and extrapolate up to $q^2 \simeq 6$ GeV^2. More precisely, (20) corresponds to a parametrization of the type $|\Delta C_9^i| = 2m_b m_B/q^2 \delta_{i1} + \delta_{i2}$, and the fits give $\delta_{11} = 0.02$, $\delta_{12} = 0.18$, $\delta_{31} = 0.03$, $\delta_{32} = 0.78$. This correction is implemented numerically in this work as a flat error in the corresponding helicity amplitudes. The contribution r_+ is additionally power suppressed as discussed above, and we will use the same parameters as in r_- but multiplied by Λ/m_B.

In Fig. 4 we also show the parametrization used in [79] as (blue) dashed lines, where the partonic result is matched to a hadronic representation via a dispersion integral and a model for the continuum contribution. This is shown as an illustration of the possible large long-distance effects that could be induced by the Q_1^c and Q_2^c operators at $q^2 \gtrsim 6$ GeV^2 and whose description requires introducing model dependence. This is also consistent with the findings of Ref. [37].

Other contributions to r_λ can also be investigated. Those induced by the chromomagnetic penguin operator Q_8 have been studied in the context of LCSR in [84] and [85], an their contributions turn out to be very small. The contributions involving light-quark loops can be problematic at low q^2 since their treatment in QCDF is the dual to the one induced by light vector resonances. However, they always

[5]We stress that the gluon is soft in the B rest frame. This is different from the case where one considers extra collinear gluons, such as in deriving a light-cone sum rule with K^* distribution amplitudes; see the discussion in [33]. However, as explained, it is soft gluon emission that determines power corrections incalculable in QCD factorization.

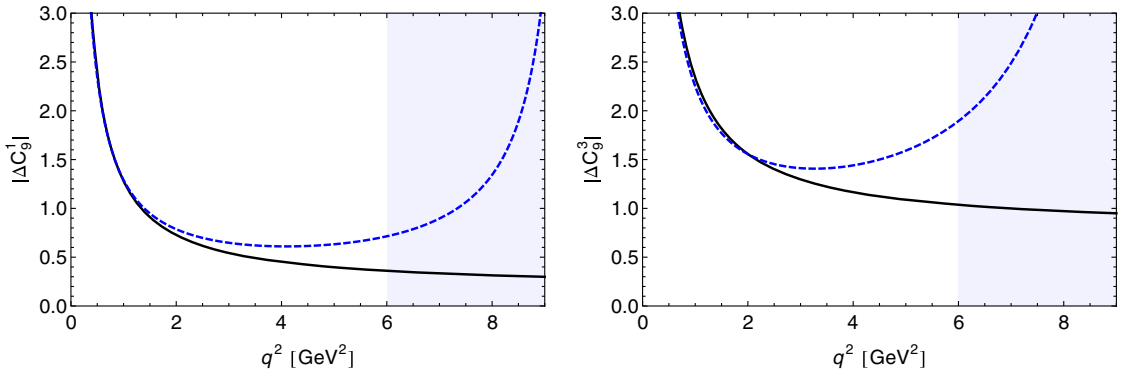

FIG. 4. Long-distance charm contributions parametrized as a correction to the Wilson coefficient C_9. The (black) solid line results from the maximum possible contribution as shown in Ref. [79]. We show the modulus of the (complex) correction extrapolated up to $q^2 \simeq 6$ GeV^2. The (blue) dashed lines correspond to the hadronic parametrization used in [79].

come doubly CKM suppressed or multiplied by small Wilson coefficients. A study of the impact of the duality violation (in relation to the QCDF result) was done using vector-meson dominance in [33] and it turned out to be negligibly small in the binned angular observables. It was also shown that $r_+^{u,d,s}$ for the light quarks is also suppressed by $(\Lambda/m_B)^2$.

For all this, we neglect the power corrections to the other terms, effectively absorbing them into r_λ^c and will treat all the corrections to r_+ suppressed by $(\Lambda/m_B)^2$.

III. ANGULAR OBSERVABLES AND THE ANALYSIS OF THE EXPERIMENTAL DATA

The q^2-dependent angular distribution (summed over lepton spins) is quadratic in the helicity amplitudes and has been given in [33]. Certain ratios of angular coefficients are favored because of their reduced sensitivity to form factors. In particular, we will discuss the so-called $P_i^{(\prime)}$ basis which was introduced in [23,31]. This is an exhaustive set of observables, constructed from ratios of the angular coefficients and engineered to cancel most of the hadronic uncertainties in the HQ/LE limit.

In order to illustrate this and critically reexamine the residual uncertainties on those observables, we will focus on two of them, called P_1 and P_5' in [23,31]. In terms of the helicity amplitudes, they read:

$$P_1 = \frac{-2\mathrm{Re}(H_V^+ H_V^{-*} + H_A^+ H_A^{-*})}{|H_V^+|^2 + |H_V^-|^2 + |H_A^+|^2 + |H_A^-|^2}, \tag{21}$$

$$P_5' = \frac{\mathrm{Re}[(H_V^- - H_V^+)H_A^{0*} + (H_A^- - H_A^+)H_V^{0*}]}{\sqrt{(|H_V^0|^2 + |H_A^0|^2)(|H_V^+|^2 + |H_V^-|^2 + |H_A^+|^2 + |H_A^-|^2)}} \tag{22}$$

where we have neglected the muon mass for clarity and have introduced the short-hand notation $H_{V,A}(\lambda) = H_{V,A}^\lambda$.

In certain approximations P_1 and P_5' become free of nonperturbative uncertainties. In the HQ/LE limit and neglecting α_s corrections, as well as the contributions h_λ from the hadronic weak Hamiltonian, the $\lambda = +$ helicity amplitudes vanish and $V_\lambda(q^2) = T_\lambda(q^2)$. As a result, in these limits and in the SM,[6]

$$P_1 = 0, \tag{23}$$

$$P_5' = \frac{\mathrm{Re}[C_{10}^* C_{9,\perp} + C_{9,\parallel}^* C_{10}]}{\sqrt{(|C_{9,\parallel}|^2 + |C_{10}|^2)(|C_{9,\perp}|^2 + |C_{10}|^2)}}, \tag{24}$$

where $C_{9,\perp} = C_9^{\mathrm{eff}}(q^2) + \frac{2m_b m_B}{q^2} C_7^{\mathrm{eff}}$, $C_{9,\parallel} = C_9^{\mathrm{eff}}(q^2) + \frac{2m_b}{m_B} C_7^{\mathrm{eff}}$, and the $P_i^{(\prime)}$ are functions of the Wilson coefficients alone.

Thus, the leading sources of uncertainties for the observables in the $P_i^{(\prime)}$ basis are due to the presence of nonfactorizable contributions as well as to corrections to the HQ/LE form factor relations. To see this explicitly, note that

$$\begin{aligned} P_5' = P_5'|_\infty \Bigg(& 1 + \frac{a_{V_-} - a_{T_-}}{\xi_\perp} \frac{m_B}{|\vec{k}|} \frac{m_B^2}{q^2} C_7^{\mathrm{eff}} \\ & \times \frac{C_{9,\perp} C_{9,\parallel} - C_{10}^2}{(C_{9,\parallel}^2 + C_{10}^2)(C_{9,\perp} + C_{9,\parallel})} + \frac{a_{V_0} - a_{T_0}}{\xi_\parallel} 2C_7^{\mathrm{eff}} \\ & \times \frac{C_{9,\perp} C_{9,\parallel} - C_{10}^2}{(C_{9,\parallel}^2 + C_{10}^2)(C_{9,\perp} + C_{9,\parallel})} + 8\pi^2 \frac{\tilde{h}_-}{\xi_\perp} \frac{m_B}{|\vec{k}|} \frac{m_B^2}{q^2} \\ & \times \frac{C_{9,\perp} C_{9,\parallel} - C_{10}^2}{C_{9,\perp} + C_{9,\parallel}} + \text{further terms} \Bigg) + \mathcal{O}(\Lambda^2/m_B^2), \end{aligned} \tag{25}$$

[6]We will ignore in this discussion the strange quark mass which produces an effect suppressed by m_s/m_b in P_1.

where for simplicity we have assumed real Wilson coefficients, $\tilde{h}_+$ denotes the nonlocal term h_λ with its leading term removed (absorbed into $C_9^{\rm eff}$), and we have neglected the difference between m_b and m_B as a higher-order effect. We see in the second term on the first line the presence of the power correction combination $a_{V_-} - a_{T_-}$. This is invariant under change of soft form factor scheme [cf. (9)]—in particular it does not matter whether V_- or T_- is identified with $\xi_\perp$, implying $a_{V_-} = 0$ or $a_{T_-} = 0$, respectively. Similarly, power corrections to the helicity-zero form factors enter only in the combination $(a_{V_0}—a_{T_0})$ (second line). Both can be understood by observing that form factors cancel out of P_5' completely if $C_7^{\rm eff}$, the $\lambda = +$ amplitudes, and nonfactorizable corrections are all neglected. As a result, form factor uncertainties enter only through interference of the tensor and vector form factors, and of form factors and nonfactorizable corrections. Put another way, form factor uncertainties enter the P_i only through deviations of the form factor differences $T_\lambda - V_\lambda$ from their zero HQ/LE limit. (For $\lambda = -, 0$, these could be traded for the deviations of the ratios T_λ/V_λ from one.) At the model-independent level, lacking first-principles results on the individual form factors all one can achieve is to parametrize the power correction $T_\lambda - V_\lambda$ in some way. For example, without loss of generality one can parametrize

$$T_-(q^2) - V_-(q^2) \equiv a_{T_-} + b_{T_-}\frac{q^2}{m_B^2} + \cdots$$

$$\text{(corresponding to } a_{V_-} = 0\text{)}$$

or one can take

$$T_-(q^2) - V_-(q^2) \equiv -a_{V_-} - b_{V_-}\frac{q^2}{m_B^2} + \cdots$$

$$\text{(corresponding to } a_{T_-} = 0\text{)}.$$

This is an equivalent way of defining the same power correction schemes discussed above. Clearly, any model prediction such as a sum rule calculation can be expressed in either parametrization. Of course, the prediction for a physical observables does not depend on which choice is made, as the scheme dependence of the model calculation cancels against that in the observable calculation (in the present case, simply a_{T_-} and $-a_{V_-}$ are traded for one another in the intermediate stages, and similarly b_{T_-} and $-b_{V_-}$).

The interference is most important if $C_7^{\rm eff}$ and $C_9^{\rm eff}(q^2)$ are comparable, as happens in particular around the zero-crossing of P_5'. The term displayed on the last line involves nonfactorizable corrections. All three terms demonstrate how the soft form factors with their associated uncertainties re-enter at subleading power. The full expression is quite lengthy and depends on all power-correction parameters and the three nonlocal terms. A similar sensitivity to power corrections occurs in most of the other angular coefficients, and in the observables in the $P_i^{(\prime)}$ basis built from them. This includes the locations of the zero-crossings of these observables.

In striking contrast, the $\mathcal{O}(\Lambda/m_B)$ power corrections to P_1 take the simple form

$$\begin{aligned} P_1 = \frac{1}{C_{9,\perp}^2 + C_{10}^2}\frac{m_B}{|\vec{k}|}\Bigg(& -\frac{a_{T_+}}{\xi_\perp}\frac{2m_B^2}{q^2}C_7^{\rm eff}C_{9,\perp} \\ & -\frac{a_{V_+}}{\xi_\perp}(C_{9,\perp}C_9^{\rm eff} + C_{10}^2) - \frac{b_{T_+}}{\xi_\perp}2C_7^{\rm eff}C_{9,\perp} \\ & -\frac{b_{V_+}}{\xi_\perp}\frac{q^2}{m_B^2}(C_{9,\perp}C_9^{\rm eff} + C_{10}^2) + 16\pi^2\frac{h_+}{\xi_\perp}\frac{m_B^2}{q^2}C_{9,\perp}\Bigg) \\ & + \mathcal{O}(\Lambda^2/m_B^2). \end{aligned} \tag{26}$$

Apart from depending on only one soft form factor and fewer power-correction and nonlocal parameters, these terms suffer further suppression: a_{T_+} vanishes exactly as discussed in Sec. II A 1, the next three terms are suppressed by a power of q^2/m_B^2 relative to the denominator at small q^2, and h_+ has an extra power suppression as discussed in the previous section. As a result, P_1 vanishes like $\mathcal{O}(\Lambda^2/m_B^2)$, $\mathcal{O}(C_9^{\rm eff}/C_7^{\rm eff} \times q^2/m_B^2 \times \Lambda/m_B)$ at small q^2 in the SM. By contrast, in the presence of nonzero C_7' it is order one. Analogous is the case of the CP-asymmetry P_3^{CP} [20,33], which at low q^2 cleanly probes a BSM weak phase in C_7'.

Finally let us comment on the extension of our conclusions to the observables in the S_i basis, where the total decay rate is used to normalize the angular observables [14]. The theoretical errors are in general expected to be larger than in the $P_i^{(\prime)}$ basis, because the sensitivity to $\xi_\perp(q^2)$ and $\xi_\parallel(q^2)$ is enhanced in the heavy-quark limit without the P_i' basis optimization. However, the suppression in the SM of the $\lambda = +$ amplitudes still implies the same $\mathcal{O}(\Lambda^2/m_B^2)$, $\mathcal{O}(C_9^{\rm eff}/C_7^{\rm eff} \times q^2/m_B^2 \times \Lambda/m_B)$ suppression seen above for the "un-optimized" versions of P_1 and P_3^{CP}, S_3 and A_9, respectively, and the additional form factor uncertainties affect only the normalization of the residual term in these two special cases, which is very small at small q^2.

A. Statistical framework and predictions in the SM

In the analysis of experimental data one must specify the treatment of the theoretical uncertainties in the statistical framework to be used. A frequentist scheme that has been successfully applied to the analysis of the CKM unitarity triangle by the *CKMfitter* collaboration is the range fit (or *R*fit) method [86]. In this approach, the χ^2 is first constructed in the usual way, based on a vector of experimentally measured observables $\vec{x}$ with

TABLE I. Results for the bin $[1,6]$ GeV^2 in the SM for a selection of observables and using different schemes for the estimation of the theoretical uncertainties. We compare with independent calculations in the literature [30,38,52] whenever it is possible. In the last column we show the experimental data.

	Max. spread	Max. spread (V_- and V_0)	1σ Gaussian	Ref. [30,52]	Ref. [38]	Expt.
P_1	$-0.03^{+0.22}_{-0.24}$	$-0.03^{+0.22}_{-0.23}$	$-0.03^{+0.13}_{-0.13}$	—	$0.009^{+0.038}_{-0.044}$	0.15(40)
P_2	$-0.12^{+0.41}_{-0.37}$	$-0.11^{+0.37}_{-0.33}$	$-0.10^{+0.19}_{-0.19}$	$-0.15^{+0.07}_{-0.07}$	$-0.21^{+0.17}_{-0.20}$	$-0.66(23)$
P_5'	$-0.36^{+0.45}_{-0.34}$	$-0.37^{+0.40}_{-0.34}$	$-0.36^{+0.19}_{-0.17}$	$-0.34^{+0.09}_{-0.08}$	$-0.41^{+0.11}_{-0.12}$	0.21(21)

experimental uncertainty $\vec{\sigma}$.[7] The theoretical determination of the observables depends on two types of variables: (i) A set $\vec{C}$ of short-distance Wilson coefficients of the effective weak Hamiltonian; (ii) hadronic parameters, $\vec{y}$ that can be determined using various nonperturbative methods with some systematic uncertainty $\vec{\delta}$. A piece is then added to the χ^2 that does not contribute unless any of the components y_i leaves the range determined by its uncertainty, δ_i. More explicitly:

$$\chi^2(\vec{C},\vec{y}) = \begin{cases} \sum_i \frac{(x_i - x_i^{\rm th}(\vec{C},\vec{y}))^2}{\sigma_i^2}, & \text{if } y_k \in [\bar{y}_k - \delta_k, \bar{y}_k + \delta_k] \quad \forall k \\ \infty, & \text{otherwise} \end{cases}. \tag{27}$$

Once it is in this form, one can treat the set $\vec{y}$ as nuisance parameters to construct a "profile χ^2" depending on the Wilson coefficients alone,

$$\tilde{\chi}^2(\vec{C}) = \min_{\vec{y}} \chi^2(\vec{C},\vec{y}), \tag{28}$$

and determine confidence level (C.L.) intervals for the C_i in a frequentist fashion and irrespective of the values of the other QCD parameters. Obviously, QCD parameters with particular interest, e.g. for testing nonperturbative calculations, can be promoted to the set of "interesting" parameters in $\vec{C}$ and be determined simultaneously from the experimental data.

Another statistical framework would be to implement the theoretical uncertainties in a χ^2 by adding in quadratures to the experimental uncertainties [50,53,54]. This implicitly assumes that the theoretical errors distribute normally or can be measured independently, although this will be rarely the case.

These considerations have to be kept in mind when interpreting the theoretical predictions of the observables. In particular, it is clear that the *R*fit method scans the space of parameters $\vec{y}$ within the interval defined by its uncertainty, searching for C.L. intervals that maximize the agreement between theory and experimental data. Thus, our uncertainties must be interpreted in terms of the maximal spread of theoretical predictions that will be considered in the global fits. On the other hand, it is important to stress that the nuisance parameters are also implicitly fitted and the range of their values will be further constrained in the analysis.

In the first three columns of Table I we show the results produced in the SM using the model-independent approach described in Sec. II A. The relevant input parameters with their uncertainties are listed in Table II, while for the Wilson coefficients in the SM we use NNLL accuracy [87]. The central values in the two first columns correspond to those of the parameters and the errors to the maximum spread produced by the scan within the range produced by their uncertainties. In the second column, we employ a different parametrization for the soft form factors. Instead of T_- and S, and following the approach suggested in [38], we choose $\xi_\perp = m_B/(2E)V_-$ and $\xi_\parallel = V_0$ to study the effect on the uncertainties introduced by these choices. Equation (11) and the values of the parameters in (13) and (15) also hold in this case. In the third column, we show the results assuming that the parameters $\vec{y}$ are normally distributed and uncorrelated, and we quote the mean and the 1σ C.L. of the distributions resulting for the observables.

From the results of the two first columns, we conclude that different identifications of the soft form factors to the QCD ones can produce small differences in the results, which can be reconciled with reasonable changes in the power-correction parameters a_X and b_X. As stressed in

TABLE II. Input parameters employed in the calculations of this work. Values for the soft form factors and power-correction parameters is found in Sec. II A.

$m_{b,(1S)}$	4.65(3) [88]	$\alpha_s(M_Z)$	0.1184(7) [88]
m_c	1.275(25) [88]	f_{K^*}	220(5) MeV [33]
m_s	0.095(5) [88]	$f_{K^*\perp}$	170(20) MeV [33]
λ	0.22543(77) [89]	a_1	0.2(2) [5]
A	0.812(19) [89]	a_2	0.1(3) [5]
$\bar{\rho}$	0.145(27) [89]	f_B	0.1905(42) GeV [90]
$\bar{\eta}$	0.343(15) [89]	$\lambda_{B,+}^{-1}$	2.0(5) GeV^{-1} [5]

[7]The correlations for the data used in this paper have not been published and we assume in our fits that the different measurements are uncorrelated.

TABLE III. Binned results in the SM for the branching fraction, the longitudinal polarization fraction F_L and the angular observables in the $P_i^{(\prime)}$ basis (using the LHCb conventions [45,49]). For the electronic mode we give predictions for the bin $[0.0020^{+0.0008}_{-0.0008}, 1.12^{+0.06}_{-0.06}]$ [91].

Bin [GeV^2]	Br $[10^{-8}]$	F_L	P_1	P_2	P_3^{CP} $[10^{-4}]$	P_4'	P_5'	P_6'	P_8'
[0.1, 0.98]	$8.6^{+4.5}_{-3.1}$	$0.26^{+0.21}_{-0.14}$	$0.03^{+0.06}_{-0.05}$	$-0.175^{+0.039}_{-0.041}$	$0.2^{+1.1}_{-0.8}$	$0.19^{+0.06}_{-0.08}$	$0.56^{+0.13}_{-0.14}$	$0.04^{+0.08}_{-0.08}$	$0.00^{+0.09}_{-0.09}$
[1.1, 2]	$3.4^{+2.9}_{-1.5}$	$0.68^{+0.17}_{-0.23}$	$0.04^{+0.11}_{-0.11}$	$-0.83^{+0.16}_{-0.09}$	$0.4^{+3.4}_{-2.3}$	$0.04^{+0.16}_{-0.18}$	$0.35^{+0.30}_{-0.32}$	$0.06^{+0.19}_{-0.19}$	$0.01^{+0.11}_{-0.11}$
[2, 3]	$3.4^{+3.4}_{-1.5}$	$0.78^{+0.13}_{-0.21}$	$0.01^{+0.12}_{-0.15}$	$-0.84^{+0.39}_{-0.14}$	$0.4^{+4.3}_{-2.9}$	$-0.19^{+0.23}_{-0.20}$	$-0.10^{+0.47}_{-0.42}$	$0.06^{+0.26}_{-0.27}$	$0.02^{+0.09}_{-0.09}$
[3, 4]	$3.6^{+3.8}_{-1.8}$	$0.77^{+0.14}_{-0.24}$	$-0.03^{+0.27}_{-0.27}$	$-0.21^{+0.50}_{-0.53}$	$0.3^{+3.4}_{-2.6}$	$-0.37^{+0.23}_{-0.16}$	$-0.49^{+0.52}_{-0.36}$	$0.05^{+0.27}_{-0.28}$	$0.01^{+0.06}_{-0.06}$
[4, 5]	$4.0^{+4.3}_{-2.1}$	$0.73^{+0.18}_{-0.28}$	$-0.06^{+0.34}_{-0.32}$	$0.30^{+0.35}_{-0.52}$	$0.2^{+2.3}_{-2.1}$	$-0.45^{+0.20}_{-0.12}$	$-0.69^{+0.48}_{-0.30}$	$0.04^{+0.25}_{-0.26}$	$0.01^{+0.05}_{-0.05}$
[5, 6]	$4.6^{+5.1}_{-2.6}$	$0.68^{+0.22}_{-0.30}$	$-0.07^{+0.39}_{-0.38}$	$0.59^{+0.23}_{-0.40}$	$0.1^{+1.7}_{-1.6}$	$-0.48^{+0.17}_{-0.10}$	$-0.80^{+0.43}_{-0.27}$	$0.03^{+0.23}_{-0.24}$	$0.01^{+0.05}_{-0.06}$
[1.1, 6]	19^{+19}_{-9}	$0.73^{+0.17}_{-0.25}$	$-0.02^{+0.23}_{-0.24}$	$-0.10^{+0.41}_{-0.39}$	$0.3^{+2.7}_{-1.9}$	$-0.30^{+0.21}_{-0.16}$	$-0.38^{+0.46}_{-0.34}$	$0.05^{+0.24}_{-0.25}$	$0.01^{+0.06}_{-0.05}$
Electron	23^{+10}_{-8}	$0.12^{+0.14}_{-0.07}$	$0.03^{+0.05}_{-0.05}$	$-0.080^{+0.017}_{-0.016}$	$0.3^{+1.0}_{-0.7}$	$0.19^{+0.06}_{-0.07}$	$0.52^{+0.12}_{-0.12}$	$0.04^{+0.07}_{-0.07}$	$0.00^{+0.08}_{-0.08}$

Sec. II A 1, this comparison provides a test of self-consistency to any approach based on the HQ/LE limit. Therefore, it is surprising that the opposite conclusion was drawn from the similar analysis of Ref. [38]. By comparing the results obtained in the first and third columns we observe that treating the theoretical errors as normally distributed one obtains, at 1σ, less than $1/2$ the uncertainty produced by the scan of the parameter space.

In the fourth and fifth columns of Table I, we show the results of independent calculations, Refs. [30] (Bayesian) and [38], respectively, and in the last column, the LHCb data. The predictions from Ref [52] (nominal priors) are the result of a Bayesian treatment assuming normal distributions for the nuisance parameters. The description of the power corrections is different to the one employed in this work. A scale factor is introduced at the level of the amplitudes [13] that is normally distributed around 1 and with the standard deviation at the 0.15%. However note that with this method the corrections to the relation $T_\lambda(q^2) = V_\lambda(q^2)$ are omitted and, as discussed in Sec. III, the uncertainties in observables like P_5' or P_2 could be underestimated at low q^2. On the other hand, Ref. [38] (KMPW scheme) uses a parametrization of the power corrections to the form factors similar to the one proposed here, and quotes the maximum spread of theoretical predictions. However the power-correction parameters are not treated as uncertainties constrained only by model-independent relations but they are in part fitted to LCSR calculations.

We finish the comparison by noting that the uncertainties have increased as compared to our previous work in Ref. [33]. This is largely explained by the improved treatment of the nonfactorizable soft contributions used in this paper and, to a lesser extent, by the different values used for the power-corrections parameters and $\xi_\perp(0)$. Also, in the present analysis, we scan all parameters simultaneously, whereas in Ref. [33] they were separated in four groups and added in quadratures.

B. Predictions for $B \to K^* \mu^+ \mu^-$ and $B \to K^* e^+ e^-$ angular observables

In Table III, we update our predictions in the SM and the muonic mode for the branching fraction, the longitudinal polarization fraction F_L and the angular observables in the $P_i^{(\prime)}$ basis (defined using the LHCb conventions [45,49]), in the narrow binning scheme. We also show predictions for

TABLE IV. Binned results in the SM for the branching fraction, the longitudinal polarization fraction F_L and the angular observables in the $P_i^{(\prime)}$ basis (using the LHCb conventions [45,49]). The results are obtained using Montecarlos in which the nuisance parameters are distributed normally and we quote for each case the mean as central value and the 1σ intervals as error bars. For the electronic mode we give predictions for the bin $[0.0020^{+0.0008}_{-0.0008}, 1.12^{+0.06}_{-0.06}]$ [91].

Bin [GeV^2]	Br $[10^{-8}]$	F_L	P_1	P_2	P_3^{CP} $[10^{-4}]$	P_4'	P_5'	P_6'	P_8'
[0.1, 0.98]	$8.5^{+2.0}_{-1.8}$	$0.26^{+0.10}_{-0.09}$	$0.025^{+0.023}_{-0.022}$	$-0.177^{+0.020}_{-0.021}$	$0.02^{+0.34}_{-0.36}$	$0.181^{+0.029}_{-0.035}$	$0.57^{+0.06}_{-0.06}$	$0.040^{+0.033}_{-0.033}$	$0.000^{+0.044}_{-0.043}$
[1.1, 2]	$3.4^{+1.1}_{-0.9}$	$0.68^{+0.10}_{-0.12}$	$0.03^{+0.05}_{-0.05}$	$-0.84^{+0.07}_{-0.06}$	$0.3^{+0.8}_{-0.8}$	$0.03^{+0.07}_{-0.08}$	$0.36^{+0.14}_{-0.14}$	$0.06^{+0.08}_{-0.08}$	$0.01^{+0.05}_{-0.05}$
[2, 3]	$3.4^{+1.4}_{-1.0}$	$0.78^{+0.07}_{-0.11}$	$0.01^{+0.06}_{-0.07}$	$-0.83^{+0.16}_{-0.10}$	$0.3^{+0.9}_{-0.7}$	$-0.20^{+0.10}_{-0.10}$	$-0.10^{+0.21}_{-0.20}$	$0.06^{+0.11}_{-0.11}$	$0.014^{+0.035}_{-0.035}$
[3, 4]	$3.6^{+1.5}_{-1.1}$	$0.78^{+0.08}_{-0.11}$	$-0.04^{+0.16}_{-0.16}$	$-0.19^{+0.24}_{-0.26}$	$0.3^{+0.9}_{-0.7}$	$-0.37^{+0.10}_{-0.08}$	$-0.49^{+0.22}_{-0.19}$	$0.05^{+0.12}_{-0.12}$	$0.013^{+0.020}_{-0.020}$
[4, 5]	$4.0^{+1.8}_{-1.2}$	$0.73^{+0.10}_{-0.13}$	$-0.05^{+0.22}_{-0.21}$	$0.32^{+0.18}_{-0.23}$	$0.2^{+0.8}_{-0.7}$	$-0.45^{+0.08}_{-0.07}$	$-0.69^{+0.20}_{-0.17}$	$0.3^{+0.12}_{-0.12}$	$0.011^{+0.017}_{-0.017}$
[5, 6]	$4.6^{+1.9}_{-1.4}$	$0.67^{+0.12}_{-0.15}$	$-0.07^{+0.24}_{-0.24}$	$0.60^{+0.12}_{-0.17}$	$0.1^{+0.6}_{-0.6}$	$-0.48^{+0.08}_{-0.06}$	$-0.80^{+0.18}_{-0.15}$	$0.02^{+0.11}_{-0.11}$	$0.01^{+0.02}_{-0.02}$
[1.1, 6]	19^{+8}_{-5}	$0.73^{+0.09}_{-0.12}$	$-0.03^{+0.14}_{-0.14}$	$-0.08^{+0.19}_{-0.20}$	$0.2^{+0.6}_{-0.5}$	$-0.31^{+0.09}_{-0.08}$	$-0.38^{+0.20}_{-0.17}$	$0.04^{+0.10}_{-0.11}$	$0.01^{+0.02}_{-0.02}$
Electron	23^{+6}_{-5}	$0.13^{+0.06}_{-0.05}$	$0.033^{+0.021}_{-0.019}$	$-0.080^{+0.008}_{-0.008}$	$0.27^{+0.32}_{-0.36}$	$0.194^{+0.026}_{-0.032}$	$0.52^{+0.05}_{-0.05}$	$0.035^{+0.027}_{-0.027}$	$0.001^{+0.042}_{-0.042}$

the electronic mode in an "effective" low-q^2 bin [91] $[0.0020^{+0.0008}_{-0.0008}, 1.12^{+0.06}_{-0.06}]$. All these predictions are obtained scanning the nuisance parameter space and extracting the maximum spread for the errors. The errors propagated from the uncertainties in the range of the bin in the electronic case are very small and neglected.

In Table IV we show instead the predictions we obtained using Gaussian distributions for the nuisance parameters, quoting the mean and the 1σ interval for the observables.

C. The $B \to K^* \mu^+ \mu^-$ anomaly

As it has been stressed above, the angular observables in $B \to K^* \ell^+ \ell^-$ at low q^2 are usually afflicted by the leading power corrections to the HQ/LE factorization formula for the decay amplitude. In order to illustrate the impact that these can have in the phenomenological analyses, we investigate the significance of the recently claimed tensions with the SM in $B \to K^* \mu^+ \mu^-$ at low q^2 and employing the model-independent approach to the nonperturbative uncertainties presented here and in Ref. [33]. As discussed in Sec. II A 2, the bin showing the largest discrepancy, $[4.3, 8.63]$ GeV^2 [49], suffers from uncertain charm-loop contributions for which no model-independent framework exists even in the heavy-quark limit, as the bin extends outside the range of validity of QCD factorization, employed both here and in [38]. Therefore, we restrict our investigation to the CP-averaged angular observables in the $P_i^{(\prime)}$ basis, augmented by the CP asymmetry P_3^{CP}, measured in the bin $[1, 6]$ GeV^2 [45,49].

On the left-hand side of Fig. 5 we show the contours for the χ^2 constructed with this angular data in the SM (all the Wilson coefficients set to their SM values), as a function of the power corrections to the vector form factors $a_{V_\pm}$ and where we have profiled over the rest of the QCD parameters. The χ^2 receives an important contribution from the measured P_5', which in our plot is represented by the overlaid diagonal contours obtained setting all the other QCD parameters to their central values. This is consistent with the conclusions of the different analyses (e.g. Ref. [50]), and we also agree that the data favors a negative NP contribution to C_9. However, in our case the significance is smaller, below 2σ, as in our approach the data can be accommodated quite well by reasonable values of the power corrections. This is shown on the right-hand side of Fig. 5, where we plot the $\Delta\chi^2$ as a function of the contribution of NP to C_9 ($\chi^2_{\rm min} \sim 1$) and where (i) we profile over all QCD parameters and (ii) set the NP contributions to all other Wilson coefficients to zero. One can explore the dependence of these results on some of our choices. In particular, we show also the χ^2 for the case in which we use (V_-, V_0) to fix the soft form factors. In this case, represented by the green dashed line, and where we have used the same estimates for the power corrections as in our standard choice, the agreement worsens somewhat, increasing the significance to close to 2σ. We emphasize, in line with our above demonstration of the form-factor scheme independence of the observables to linear order, that this increase in significance is not to be interpreted as favoring this form-factor scheme. Rather the difference in significances between the two form-factor schemes can be taken as a measure of the uncertainty due to higher-order power corrections.

The advantage of our parametrization of the power corrections is that they are related to specific QCD matrix elements and the outcome of our analysis can be compared directly to the results of nonperturbative calculations. For instance, our SM fit on the left-hand side of Fig. 5 favors a

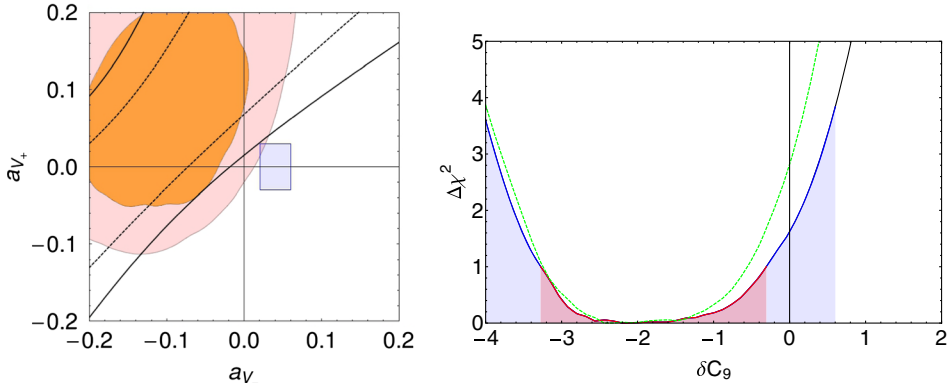

FIG. 5. Graphs for the $B \to K^* \ell^+ \ell^-$ anomaly. Left panel: 68% and 95% C.L. bounds in the parameter space of the power corrections $a_{V_\pm}$ and for a fit in the SM. We use a profile χ^2 including only the $P_i^{(\prime)}$ observables in the bin $[1, 6]$ GeV^2. The origin of the axis corresponds to QCDF and the small dashed box corresponds to the subspace for the LCSR of Ref. [78] when the errors of V and A_1 are combined linearly. Right panel: Profile χ^2 including only the angular observables in the $P_i^{(\prime)}$ basis in the bin $[1, 6]$ GeV^2 as a function of a BSM contribution to C_9 and setting all the other Wilson coefficients to their SM values. The red and blue shades indicate the limits for the 68% and 95% C.L. The dashed green line corresponds to the case in which V_- and V_0 are used to fix the soft form factors. In both cases $\chi^2_{\rm min} \sim 1$.

value of a_{V_-}, more generally of $a_{V_-} - a_{T_-}$ or equivalently a correction to the ratio $V^{\infty}(0)/T^{\infty}(0)$ computed in QCDF, that is negative. However, as it was advanced in Sec. II A 1, this is a scenario that is not compatible with the LCSR calculation of Ref. [78], where the correction is obtained with the opposite sign. This is illustrated by the blue box in the plot, which describes the size of the power corrections predicted by the LCSR and estimated as described in Sec. II A 1.

In conclusion, the interpretation $B \to K^* \mu^+ \mu^-$ anomaly is blurred by the sensitivity of the relevant observables to power corrections. From the discussion above it is clear that implementing the QCD form factors in the LCSR enhances the signal and that a careful assessment of the accuracy of the various nonperturbative approaches seems to be still necessary to unambiguously attribute this anomaly to NP (for some recent developments within LCSR see [92]).

D. Constraints on right-handed currents

In Secs. II A and III, we argued that the angular observables P_1 and P_3^{CP} stand out among the others because they are sensitive to H_V^+. This makes them zero in the SM, up to subleading power corrections or up to leading ones that are further suppressed by a factor q^2/m_B^2. Thus, around the low q^2 end point, P_1 and P_3^{CP} are null tests of the SM in very good approximation, becoming very sensitive to right-handed currents BSM entering through the electromagnetic penguin operator Q_7'.

On the experimental side, there are the measurements of the muonic mode in the lowest-q^2 bin and those in the electronic channel, which are best due to its lower end point. Indeed, most of the difference between their branching fractions in the lowest bin shown in Table III (roughly a factor 3) stems from events in the region between the two end points. This region is especially sensitive to the physics of the photon pole and it is where the q^2/m_B^2-suppression of the leading power corrections is maximally effective. We show in Table V the error budget for the SM predictions of P_1 and P_3^{CP} in the electronic mode. As expected, the contribution to the uncertainty from the power corrections to the form factors is very small and the final theoretical error is dominated by the $(\Lambda/m_B)^2$-suppressed long-distance charm, r_+^c.

The radiative decays are also obvious probes of the structure of the electromagnetic operators and strategies to determine the helicity of the photon (and therefore C_7') with these decays have been intensively investigated [83,93–99]. The inclusive $b \to s\gamma$ decay ratio, while theoretically clean, depends only quadratically on C_7'. However, interference between helicity amplitudes (and linear dependence on C_7') can be induced by B^0-$\bar{B}^0$ mixing and the time-dependent CP-asymmetry in $B \to K^*\gamma$ and has been suggested as a clean null test of the SM [93], via its sine coefficient given by

$$S_{K^*\gamma} = \frac{2\mathrm{Im}[e^{-2i\beta}(H_-^* \bar{H}_- + H_+^* \bar{H}_+)]}{|H_+|^2 + |H_-|^2 + |\bar{H}_+|^2 + |\bar{H}_-|^2}, \tag{29}$$

where H_λ ($\bar{H}_\lambda$) corresponds to the helicity amplitudes of $B \to K^*\gamma$ ($\bar{B} \to \bar{K}^*\gamma$) and β is the angle of the CKM unitarity triangle. These helicity amplitudes are given in terms of the residues at $q^2 = 0$ of those of the semileptonic decay, $H_V(\lambda)$, cf. Eq. (3), and inherit the multiple suppression of H_V^+ in the SM. Applying the approach described in this paper for the theoretical description of the amplitudes one obtains, in the SM:

$$S_{K^*\gamma} = -0.02^{+0.016}_{-0.023}, \tag{30}$$

which is to be compared with the average of experimental measurements, $S_{K^*\gamma} = -0.16 \pm 0.22$ [100–102].

In Fig. 6 we display contour plots in the C_7' plane. On the left-hand side, we show the ideal bounds obtained for the central values of the theoretical parameters and assuming an experimental precision of 0.25 for P_1 and P_3^{CP} in both the electronic and muonic channels. We also show the constraint obtained from the current measurements of $S_{K^*\gamma}$. On the right-hand side, we show the current bound that is obtained using all the available experimental data of $B \to K^* \ell^+ \ell^-$ in the lower bins [0.1,2] and [2, 4.3] GeV^2 and of $B \to K^*\gamma$. We also use the branching fraction of $B \to X_s\gamma$, $\mathcal{B}(B \to X_s\gamma)$ that, depending quadratically on C_7', becomes the dominant contribution to the χ^2 for large values of the coefficient. We profile over all the QCD parameters, and we set all the other Wilson coefficients to their SM values.

We conclude that P_1 and P_3^{CP} conform, in combination with $S_{K^*\gamma}$ and $\mathcal{B}(B \to X_s\gamma)$, and neglecting NP contributions to the phase of the B_d mixing amplitude, a basis of clean observables that completely determine C_7 and C_7' from experiment, with the simple expressions given in [98,99] being protected from QCD uncertainties to a high degree.

With the small theoretical uncertainties in the SM predictions, one expects that the determination of these Wilson coefficients will be dominated by the experimental errors. In this regard, and as shown in the left-hand panel of Fig. 6, the measurements provided by the electronic mode are very promising. It is also worth pointing out in the right-hand panel of Fig. 6 the small discrepancy with the SM in

TABLE V. Error budget for the P_1 and P_3^{CP} for the electronic mode in the bin $[0.002, 1.12]$ GeV^2.

	Result	QCDF	Fact. p.c.'s	Nonfact. p.c.'s
P_1	$0.032^{+0.055}_{-0.048}$	$^{-0.003}_{+0.010}$	± 0.012	$^{+0.031}_{-0.029}$
P_3^{CP} $[10^{-4}]$	$0.3^{+1.0}_{-0.7}$	$^{+0.5}_{-0.2}$	$^{+0.1}_{-0.2}$	$^{+0.6}_{-0.4}$

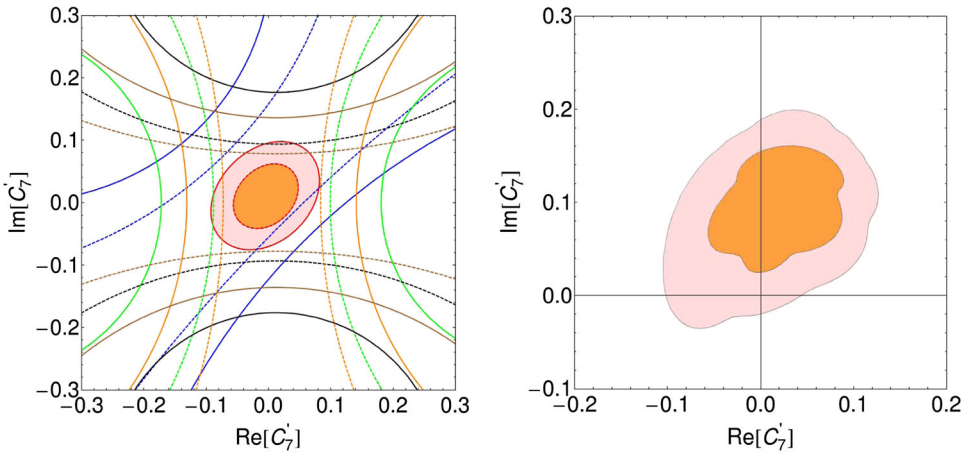

FIG. 6. Bounds in the C_7' plane. Left panel: Ideal 68% and 95% contour plots for the central values of the theoretical parameters. The diagonal band corresponds to the $S_{K^*\gamma}$ measurement and the vertical and horizontal ones to hypothetical null measurements of P_1 and P_3^{CP}, respectively, with an assumed experimental precision of 0.1. The green and black lines are for the muonic mode and the brown and orange for the electronic one. Right panel: Current bounds at 68% and 95% C.L. in the C_7' plane using all the current data of $B \to K^*\mu^+\mu^-$ in the lower bins [0.1,2] and $[2, 4.3]$ GeV^2 and of $B \to K^*\gamma$ and $B \to X_s\gamma$. We use the profile likelihood method and set all other Wilson coefficients to their SM values.

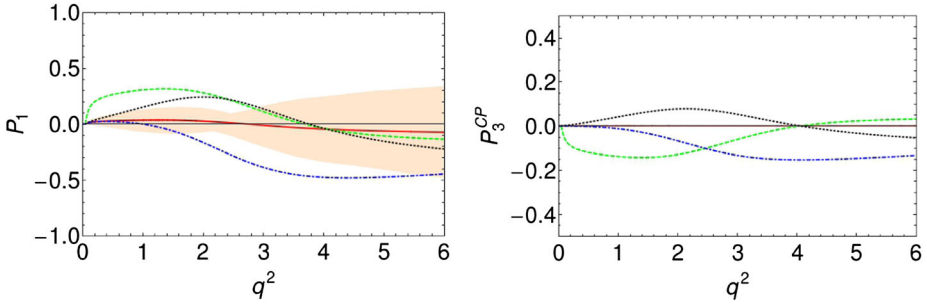

FIG. 7. Sensitivity of $P_1(q^2)$ and $P_3^{CP}(q^2)$ to right-handed quark currents. The SM predictions are the solid (red) lines and the theoretical uncertainty, represented by the band, is obtained taking the maximum spread of theoretical predictions. In the plot of $P_1(q^2)$ the NP scenarios correspond to $C_7' = -0.05$ (dashed green), $C_9' = -1$ (dotted black) and $C_{10}' = 1$ (dot-dashed blue). In the plot of $P_3^{CP}(q^2)$, we show $C_7' = -0.05$ (dashed green), $C_9' = -1$ (dotted black) and $C_{10}' = 1$ (dot-dashed blue). In the plot of $P_3^{CP}(q^2)$, we plot $C_7' = 0.05i$ (dashed green), $C_9' = -e^{i\frac{\pi}{4}}$ (dotted black) and $C_{10}' = e^{i\frac{\pi}{4}}$ (dot-dashed blue).

the imaginary part that is driven by the current measurement of the angular observable A_9 in the muonic mode.[8]

At higher q^2, P_1 and P_3^{CP} are also affected by $\mathcal{O}(\Lambda/m_B)$ power corrections induced, in this case, chiefly by the vector form factor $V_+(q^2)$. However, given their specific sensitivity to right-handed quark currents they could also serve to probe C_9' and C_{10}', especially if these are as large as recently discussed in the literature [54]. In order to demonstrate this we show in Fig. 7 the q^2 dependence of P_1 and P_3^{CP} in the SM and compared to the results in different scenarios of NP involving corrections to C_9' and C_{10}' of order 1. As discussed in Sec. III A, the correlations with other observables in terms of the same relevant QCD parameters (cf. a_{V_+}) will increase the sensitivity of P_1 and P_3^{CP} to C_9' and C_{10}' in the global fits.

IV. LEPTON-UNIVERSALITY RATIOS

In light of the recent hints on lepton universality violation (LUV) in various $b \to s\ell\ell$ measurements it becomes important to investigate the opportunities that $B \to K^*\ell\ell$ offers for the confirmation and characterization of the effect. In fact, one can introduce lepton universality ratios involving the muonic and the electronic modes for a given observable. These are extremely clean since up to kinematical $\mathcal{O}(m_\mu^2/q^2)$ corrections, they are equal to 1 in the SM and in lepton-universal NP scenarios. Let us start defining the ratio of the rates [103]:

[8]Since this discussion is meant to be an illustration of the impact of the approach of this paper in the phenomenology, we obtained our experimental P_3^{CP} from the measured A_9 and F_L via $P_3^{CP} = A_9/(1 - F_L)$, propagating errors quadratically and ignoring experimental correlations.

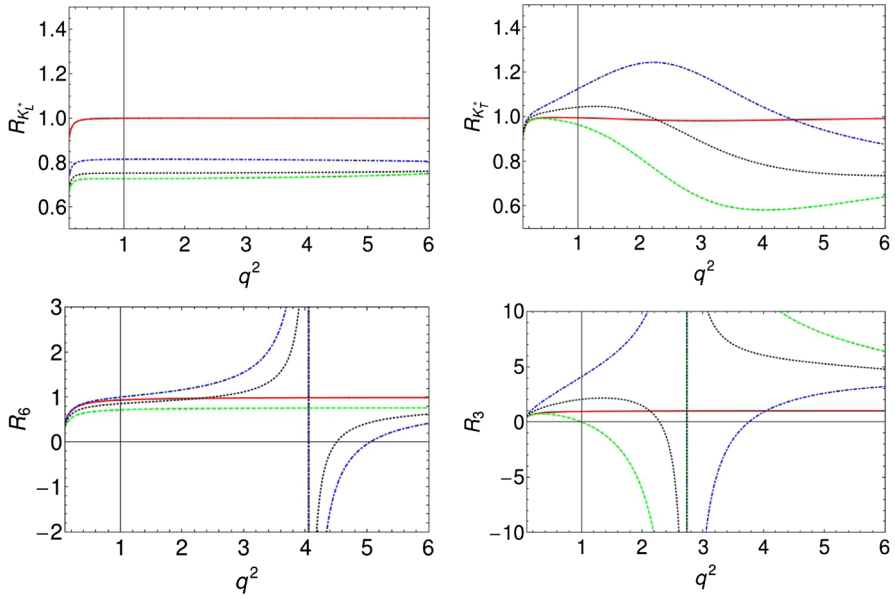

FIG. 8. Lepton-universality ratios for $B^0 \to K^{*0}\ell\ell$ in the SM and in different NP scenarios. The SM is the solid (red), A the dashed (blue), B the dot-dashed (green) and C the dotted (black) lines. In the right-hand plot of the lower panel (R_3) we show, instead, the A', B' and C' scenarios.

$$R_{K^*} = \frac{\mathcal{B}(B \to K^* \mu^+ \mu^-)}{\mathcal{B}(B \to K^* e^+ e^-)}. \tag{31}$$

Next, we can use the angular distribution of the final K and π produced in the K^* decay to separate the total $B \to K^*\ell\ell$ rate into the contributions of the decays into transversely or longitudinal K^* mesons. The balance between these two in the total decay rate is often measured by the polarization fractions $F_L = 1 - F_T$ [45]. Here we prefer to use the integrated "longitudinal" and "transversal" rates, $d\Gamma/dq^2 F_{L,T}$, and construct the corresponding lepton-universality ratios:

$$R_{K_X^*} = \frac{\mathcal{B}(B \to K_X^* \mu^+ \mu^-)}{\mathcal{B}(B \to K_X^* e^+ e^-)}. \qquad X = L, T. \tag{32}$$

Finally, one can define the ratio of the different angular observables that we define as

$$R_i = \frac{\langle \Sigma_i^\mu \rangle}{\langle \Sigma_i^e \rangle}, \tag{33}$$

where Σ_i^ℓ stands for the given observable with the leptons ℓ in the notation for the CP averages of [33] and with the brackets indicating that the angular observables have been integrated over certain q^2 region. In the discussion below, we will use the same labels for the q^2-dependent observables obtained replacing the integrated rates in Eqs. (31), (32) and (33) by the corresponding differential ones.

As it has been concluded in various analyses [56,57], the LUV signal ought to be produced by lepton-dependent semileptonic operators $Q_{9,10}^{(\prime)}$. In the following, we will discuss the lepton-universality ratios in scenarios assuming that the electronic mode is SM-like and with the NP affecting only the muonic operators. This is supported by the current (rather unprecise) electronic data set, and it would also fit a possible NP contribution to the $B \to K^* \mu^+ \mu^-$ anomaly discussed in Sec. III C [56–58,60,62,104]. Nevertheless, note that these ratios are only sensitive to the differences of the Wilson coefficients for the two leptons. We will study three scenarios: A in which $\delta C_9^\mu = -1$; B where $\delta C_{10}^\mu = -1$; and C an $SU(2)_L$-doublet scenario with $\delta C_9^\mu = -\delta C_{10}^\mu = -0.5$. As discussed in [57], these are all allowed by the LUV measurement in $B^+ \to K^+\ell\ell$. In this sense, a positive and significant NP contribution to C_{10} does not seem to be ruled out in some global analyses especially if it comes in a $SU(2)_L$ combination with C_9 [54]. In order to study plausible solutions based on quark right-handed currents, we will also consider, in one particular lepton-universality ratio, the "primed" scenarios where $\delta C_i^\mu \to \delta C_i^{\mu\prime}$.

In Fig. 8 we show a selection of the ratios (32) and (33) plotted in terms of the q^2-dependent differential rates. The first plot, on the left-hand side of the upper panel, shows the effects of the different NP scenarios on the longitudinal rate. This is analogous to the one in $B \to K\ell^+\ell^-$, and therefore a signal equivalent to the one measured in R_K should be also found in $R_{K_L^*}$. On the other hand, the effect in the ratio of the transversal rate is intrinsically different to the one probed by R_K. Indeed, $R_{K_T^*}$ depends on $|H_V^-|^2$, which includes an interference term, $C_9 C_7/q^2$, that is negative in the SM. Therefore, a contribution $\delta C_9 < 0$ is expected to reduce the interference, increasing the transversal rate at low q^2. This is what we observe on

the right-hand side of upper panel in Fig. 8, where, in the scenario A, $R_{K_T^*} > 1$ for most of the low q^2 region and up to the point where the term $|C_9^\mu|^2$ dominates and makes $R_{K_T^*} < 1$. Scenario B involves only a reduction of the quadratic term $|C_{10}^\mu|^2$ and therefore it causes an overall reduction of $R_{K_T^*}$ with respect to 1.

Besides that, the ratios R_i between different coefficients of the angular observables offer unique opportunities to investigate LUV. Some of these coefficients, like $I_6(q^2)$ (the one entering A_{FB} and P_2) and $I_5(q^2)$ (entering P_5') have zeroes at low q^2 due to the cancellations between C_9^ℓ and C_7/q^2 at work within H_V^- (see e.g. [5]). Therefore, a displacement of the zero-crossings between a muonic angular coefficient and its electronic counterpart would be also an unambiguous signal of LUV, as all long-distance QCD effects cancel out. Defining:

$$\Delta_0^i \equiv (q_0^2)_{I_i}^{(\mu)} - (q_0^2)_{I_i}^{(e)}, \tag{34}$$

an observation of a nonvanishing Δ_i^0 would provide sensitivity to LUV in $\delta C_{9\perp}$ (primarily for $i = 6$), to $\delta C_{9\perp} + \delta C_{9\parallel}$ (primarily for $i = 5$), and in addition to δC_{10} ($i = 4$).

In particular, these would manifest as singularities in the q^2 dependence of the corresponding lepton-universality ratios. As an example, we show on the left-hand side of the lower panel of Fig. 8, $R_6(q^2)$ in the SM compared to the different NP scenarios. As anticipated, in A and C, one finds singularities with the negative contributions to C_9^μ shifting the zeroes of the muonic mode to higher q^2. In scenario B, involving only a shift to C_{10}^μ, the positions of the zeroes do not change and the effect chiefly consists of a sustained (in q^2) reduction of R_6 with respect to 1. Thus, one expects that ratios R_6 taken from rates integrated up to $q^2 \simeq 4\ \mathrm{GeV}^2$ will be very sensitive to LUV entering through C_9^ℓ. A very similar plot and discussion can be made for R_5, with the exception that the zeroes of $I_5(q^2)$ are at rather lower q^2, and for R_4, whose zero is also sensitive to LUV in C_{10}^ℓ.

On the right-hand side of the lower panel of Fig. 8, we show a lepton-universality ratio, R_3, that is qualitatively different to the previous ones. The R_3 involves the same angular observable as P_1, with its strong sensitivity to right-handed currents, but with an almost exact cancellation of hadronic uncertainties in the ratio. In fact, this is shown in the plot, where the sensitivity is enhanced even more by the smallness of $I_3^\ell(q^2)$ in the SM and the fact that it has a zero which depends on C_9' and C_{10}'. This in turn also means that obtaining a useful measurement of R_3 could prove challenging as it requires non-null measurements of $I_3^\ell(q^2)$, which would already indicate NP (cf. Sec. III D) or require very high statistics.

TABLE VI. Binned predictions for the lepton-universality ratios in $B^0 \to K^{*0}\ell\ell$. Uncertainties in the SM are at the permille level.

Ratio	Bin [GeV^2]	SM	A	B	C
R_{K^*}	[0.1, 1]	0.981	0.98	0.92	0.95
	[1, 4]	0.996	0.93	0.75	0.82
$R_{K_L^*}$	[0.1, 1]	0.991	0.81	0.72	0.75
	[1, 4]	0.999	0.81	0.73	0.75
$R_{K_T^*}$	[0.1, 1]	0.979	1.02	0.97	1.00
	[1, 4]	0.987	1.18	0.79	0.97
R_6	[1, 4]	0.975	1.31	0.75	1.01

In Table VI we present various binned predictions in the SM and in the different NP scenarios discussed above. All of the latter produce a generalized reduction of $R_{K_L^*}$ by a $\sim$25%, which is equivalent to the one experienced by R_K, although now the characteristic dependence of $R_{K_T^*}$ on C_9^μ allows to distinguish among them. In A we would observe a increment of $R_{K_T^*}$, in B a 20% decrease and, in C, a value that is very similar to the SM. In fact we have chosen the bin $[1, 4]\ \mathrm{GeV}^2$ because it maximizes this sensitivity of $R_{K_T^*}$ to interference of C_9^μ with the photon pole. In anticipation to the incoming LHCb measurements of the angular observables in both, the muonic and electronic channels, we also show the results in the $[0.1, 1]\ \mathrm{GeV}^2$ bin. In this case, $R_{K_T^*}$ does not seem to be very sensitive to the NP scenarios studied, although the reduction in $R_{K_L^*}$ is similar to the one in the larger bin.

Finally, we also give results for R_6 in $[1, 4]\ \mathrm{GeV}^2$ to demonstrate the interest that measurements of the R_i ratios could have in the future. Nevertheless, we stress that the real potential of these observables lies in the measurement of their q^2 dependence. In fact, the predictions in the SM in large bins can have an *infinite* uncertainty because, for certain values of the nuisance parameters, the zeroes in I_i are such that $\langle I_i^e \rangle = 0$. This problem, of course, disappears with the measurement of R_i in a sufficiently dense array of bins.

V. CONCLUSIONS

We have revisited a model-independent approach to the nonperturbative uncertainties in $B \to K^*\ell^+\ell^-$ at large recoil [33] and in the light of the new data and recent anomalies. Our approach places the heavy-quark/large-energy limit of QCD, with its well-defined predictions and simplifications, in its core. The power corrections are parametrized incorporating only exact (model-independent) constraints in QCD. Beyond that, we treat the resulting parameters as flat errors in the amplitudes whose ranges we estimate by power-counting arguments, in case of the form factors or using explicit model calculations, for the nonfactorizable terms.

With this approach to the QCD uncertainties we intend to minimize the amount of information needed on the value and correlations of the hadronic matrix elements that should be, otherwise, obtained from nonperturbative frameworks like the light-cone sum rules. The reason for this is twofold: (i) We can classify angular observables according to their sensitivity to specific NP and hadronic effects, especially the power corrections. (ii) We make manifest the fact that the experimental data will not only test the short-distance structure of the SM but also, simultaneously, our understanding of the hadronic matrix elements involved. Therefore, in the event of a disagreement with the data and before claiming discovery of NP, it will be of utmost importance to find schemes to dissect, and hopefully rule out, the incompletely understood nonperturbative dynamics as the culprit.

We have then updated our predictions for the muonic and electronic channels and discussed various classes of observables according to their theoretical cleanness and specific sensitivities to NP. First, we demonstrated that the observables in the $P_i^{(\prime)}$ basis generally suffer from leading power corrections and argued that their theoretical uncertainties need to be carefully assessed. These conclusions extend also to the S_i basis in which the hadronic uncertainties generally do not cancel in the heavy-quark limit. We then ratified the findings of previous studies about the importance of P_5' (or S_5) in the angular analysis performed with 1 fb^{-1} of LHCb data. Our fits also favor negative NP contributions to C_9 although, contrary to the conclusions of other analyses (e.g. Refs. [50,54]), we find a pull of the angular obsevables of $B \to K^* \mu\mu$ at low q^2 (below 6 GeV^2) with respect to the SM of only about 2σ. The better consistency in our approach is achieved with an allowed region of the nuisance (QCD) parameter space that is selected by the *R*fit algorithm. Similar conclusions are obtained in the Bayesian analysis of Ref. [52] where the QCD parameters are also allowed to float in the fits. Our framework proves most useful by pointing to the specific form of the QCD hadronic matrix elements that is needed. In this sense, we discussed that agreement with the SM requires power corrections to the ratio of the tensor and vector form factors, T_- and V_-, that are not in good agreement with the ones obtained in light-cone sum rule calculations.

This discussion, in turn, emphasizes the value that two of these observables have. Indeed, P_1 and P_3^{CP} only receive contributions from the leading power corrections that are further suppressed around the low-q^2 end point, providing a theoretically clean window to right-handed currents BSM. Furthermore, the experimental prospects for the dedicated measurement of this region, especially with the electronic modes, is very promising. We argued that in combination with the radiative decays, these two observables provide a sufficient set of constraints to accurately determine the Wilson coefficients C_7' and C_7 from experiment. We determined the bounds in the C_7' plane that can be obtained with the current measurements on radiative decays and the angular observables in the muonic channel to illustrate this.

Finally, we proposed various lepton-universality ratios and relative shifts in zero-point crossings using the angular distributions of the muonic and electronic channels. These are all very accurately predicted in the SM and have a rich structure in terms of lepton-dependent Wilson coefficients. Ratios based on the transversal and longitudinal contributions to the decay rate are very useful to distinguish among different scenarios involving the semileptonic operators. In particular, $R_{K_L^*}$ is similar to the ratio in the kaonic decay, R_K, whereas $R_{K_T^*}$ shows an interesting dependence on C_9^ℓ due to the interference with the photon pole in H_V^-. Ratios involving the angular coefficient $I_{4,5,6}(q^2)$ are particularly interesting because of their zeroes that depend on C_9 and C_{10} and LUV produces the appearance of singularities in the rates. We discussed binned predictions in various NP scenarios and concluded that these lepton universality ratios have a great potential in terms of the discovery and shaping of the presumed lepton-universality interactions beyond the SM.

ACKNOWLEDGMENTS

We want to thank M. Borsato, T. Feldmann, B. Grinstein, Y. Grossman, G. Hiller, A. Khodjamirian, J. LeFrancois, Z. Ligeti, J. Matias, M. Neubert, P. Owen, K. Petridis, M.-H. Schune, D. Straub and R. Zwicky for useful discussions. S. J. acknowledges support from UK STFC under grant ST/L000504/1 and from the NExT institute. J. M. C has received funding from the People Programme (Marie Curie Actions) of the European Union's Seventh Framework Programme (FP7/2007-2013) under REA grant agreement n PIOF-GA-2012-330458 and acknowledges the Spanish Ministerio de Economía y Competitividad and European FEDER funds under the contract FIS2011-28853-C02-01 for support.

Note added.—After this work was completed and submitted, Refs. [105–107] appeared concerning BSM searches with $B \to V\ell^+\ell^-$ decays. Furthermore, Ref. [108] appeared which updates the LCSR predicions of [78]. Interestingly, while the tensor form factor $T_-(0) = T_1(0)$ in [108] is significantly lower than in [78] and now leads to a SM prediction for $BR(B \to K^*\gamma)$ in agreement with experiment, the ratio $V_-(0)/T_-(0)$ receives no significant change and remains at variance with the power corrections inferred from data (if the SM is assumed).

[1] A. Ali, T. Mannel, and T. Morozumi, Phys. Lett. B **273**, 505 (1991).
[2] G. Burdman, Phys. Rev. D **57**, 4254 (1998).
[3] D. Melikhov, N. Nikitin, and S. Simula, Phys. Lett. B **442**, 381 (1998).
[4] F. Kruger, L. M. Sehgal, N. Sinha, and R. Sinha, Phys. Rev. D **61**, 114028 (2000); **63**, 019901(E) (2000).
[5] M. Beneke, T. Feldmann, and D. Seidel, Nucl. Phys. **B612**, 25 (2001).
[6] S. W. Bosch and G. Buchalla, Nucl. Phys. **B621**, 459 (2002).
[7] A. L. Kagan and M. Neubert, Phys. Lett. B **539**, 227 (2002).
[8] T. Feldmann and J. Matias, J. High Energy Phys. 01 (2003) 074.
[9] M. Beneke, T. Feldmann, and D. Seidel, Eur. Phys. J. C **41**, 173 (2005).
[10] B. Grinstein and D. Pirjol, Phys. Rev. D **70**, 114005 (2004).
[11] F. Kruger and J. Matias, Phys. Rev. D **71**, 094009 (2005).
[12] C. Bobeth, G. Hiller, and G. Piranishvili, J. High Energy Phys. 07 (2008) 106.
[13] U. Egede, T. Hurth, J. Matias, M. Ramon, and W. Reece, J. High Energy Phys. 11 (2008) 032.
[14] W. Altmannshofer, P. Ball, A. Bharucha, A. J. Buras, D. M. Straub, and M. Wick, J. High Energy Phys. 01 (2009) 019.
[15] C. Bobeth, G. Hiller, and D. van Dyk, J. High Energy Phys. 07 (2010) 098.
[16] U. Egede, T. Hurth, J. Matias, M. Ramon, and W. Reece, J. High Energy Phys. 10 (2010) 056.
[17] A. K. Alok, A. Datta, A. Dighe, M. Duraisamy, D. Ghosh, and D. London, J. High Energy Phys. 11 (2011) 121.
[18] M. Beylich, G. Buchalla, and T. Feldmann, Eur. Phys. J. C **71**, 1635 (2011).
[19] C. Bobeth, G. Hiller, and D. van Dyk, J. High Energy Phys. 07 (2011) 067.
[20] D. Becirevic and E. Schneider, Nucl. Phys. **B854**, 321 (2012).
[21] A. K. Alok, A. Datta, A. Dighe, M. Duraisamy, D. Ghosh, and D. London, J. High Energy Phys. 11 (2011) 122.
[22] C. D. Lu and W. Wang, Phys. Rev. D **85**, 034014 (2012).
[23] J. Matias, F. Mescia, M. Ramon, and J. Virto, J. High Energy Phys. 04 (2012) 104.
[24] D. Becirevic and A. Tayduganov, Nucl. Phys. **B868**, 368 (2013).
[25] A. Y. Korchin and V. A. Kovalchuk, Eur. Phys. J. C **72**, 2155 (2012).
[26] D. Das and R. Sinha, Phys. Rev. D **86**, 056006 (2012).
[27] J. Matias, Phys. Rev. D **86**, 094024 (2012).
[28] T. Blake, U. Egede, and A. Shires, J. High Energy Phys. 03 (2013) 027.
[29] S. Descotes-Genon, D. Ghosh, J. Matias, and M. Ramon, J. High Energy Phys. 06 (2011) 099.
[30] F. Beaujean, C. Bobeth, D. van Dyk, and C. Wacker, J. High Energy Phys. 08 (2012) 030.
[31] S. Descotes-Genon, J. Matias, M. Ramon, and J. Virto, J. High Energy Phys. 01 (2013) 048.
[32] C. Bobeth, G. Hiller, and D. van Dyk, Phys. Rev. D **87**, 034016 (2013).
[33] S. Jäger and J. M. Camalich, J. High Energy Phys. 05 (2013) 043.
[34] S. Descotes-Genon, T. Hurth, J. Matias, and J. Virto, J. High Energy Phys. 05 (2013) 137.
[35] M. Dring, U. G. Meiner, and W. Wang, J. High Energy Phys. 10 (2013) 011.
[36] R. R. Horgan, Z. Liu, S. Meinel, and M. Wingate, Phys. Rev. Lett. **112**, 212003 (2014).
[37] J. Lyon and R. Zwicky, arXiv:1406.0566.
[38] S. Descotes-Genon, L. Hofer, J. Matias, and J. Virto, J. High Energy Phys. 12 (2014) 125.
[39] B. Aubert *et al.* (*BABAR* Collaboration), Phys. Rev. D **79**, 031102 (2009).
[40] B. Aubert *et al.* (*BABAR* Collaboration), Phys. Rev. Lett. **102**, 091803 (2009).
[41] J.-T. Wei *et al.* (BELLE Collaboration), Phys. Rev. Lett. **103**, 171801 (2009).
[42] J. P. Lees *et al.* (*BABAR* Collaboration), Phys. Rev. D **86**, 032012 (2012).
[43] T. Aaltonen *et al.* (CDF Collaboration), Phys. Rev. Lett. **106**, 161801 (2011).
[44] R. Aaij *et al.* (LHCb Collaboration), J. High Energy Phys. 05 (2013) 159.
[45] R. Aaij *et al.* (LHCb Collaboration), J. High Energy Phys. 08 (2013) 131.
[46] S. Chatrchyan *et al.* (CMS Collaboration), Phys. Lett. B **727**, 77 (2013).
[47] J. Schieck (ATLAS Collaboration), *Proc. Sci.*, EPS-HEP (2013) 372.
[48] T. Aaltonen *et al.* (CDF Collaboration), Phys. Rev. Lett. **108**, 081807 (2012).
[49] R. Aaij *et al.* (LHCb Collaboration), Phys. Rev. Lett. **111**, 191801 (2013).
[50] S. Descotes-Genon, J. Matias, and J. Virto, Phys. Rev. D **88**, 074002 (2013).
[51] W. Altmannshofer and D. M. Straub, Eur. Phys. J. C **73**, 2646 (2013).
[52] F. Beaujean, C. Bobeth, and D. van Dyk, Eur. Phys. J. C **74**, 2897 (2014); **74**, 3179 (2014).
[53] T. Hurth and F. Mahmoudi, J. High Energy Phys. 04 (2014) 097.
[54] W. Altmannshofer and D. M. Straub, Eur. Phys. J. C **75**, 382 (2015).
[55] R. Aaij *et al.* (LHCb Collaboration), Phys. Rev. Lett. **113**, 151601 (2014).
[56] R. Alonso, B. Grinstein, and J. M. Camalich, Phys. Rev. Lett. **113**, 241802 (2014).
[57] G. Hiller and M. Schmaltz, Phys. Rev. D **90**, 054014 (2014).
[58] D. Ghosh, M. Nardecchia, and S. A. Renner, J. High Energy Phys. 12 (2014) 131.
[59] S. Biswas, D. Chowdhury, S. Han, and S. J. Lee, J. High Energy Phys. 02 (2015) 142.
[60] T. Hurth, F. Mahmoudi, and S. Neshatpour, J. High Energy Phys. 12 (2014) 053.
[61] S. L. Glashow, D. Guadagnoli, and K. Lane, Phys. Rev. Lett. **114**, 091801 (2015).
[62] G. Hiller and M. Schmaltz, J. High Energy Phys. 02 (2015) 055.
[63] T. Iijima, Report No. DESY-PROC-2010-04.

[64] J. P. Lees *et al.* (*BABAR* Collaboration), Phys. Rev. Lett. **112**, 211802 (2014).
[65] G. Buchalla, A. J. Buras, and M. E. Lautenbacher, Rev. Mod. Phys. **68**, 1125 (1996).
[66] A. Bharucha, T. Feldmann, and M. Wick, J. High Energy Phys. 09 (2010) 090.
[67] M. J. Dugan and B. Grinstein, Phys. Lett. B **255**, 583 (1991).
[68] J. Charles, A. L. Yaouanc, L. Oliver, O. Pene, and J. C. Raynal, Phys. Rev. D **60**, 014001 (1999).
[69] M. Beneke, G. Buchalla, M. Neubert, and C. T. Sachrajda, Phys. Rev. Lett. **83**, 1914 (1999).
[70] M. Beneke, G. Buchalla, M. Neubert, and C. T. Sachrajda, Nucl. Phys. **B591**, 313 (2000).
[71] C. W. Bauer, S. Fleming, D. Pirjol, and I. W. Stewart, Phys. Rev. D **63**, 114020 (2001).
[72] C. W. Bauer, D. Pirjol, and I. W. Stewart, Phys. Rev. D **65**, 054022 (2002).
[73] M. Beneke, A. P. Chapovsky, M. Diehl, and T. Feldmann, Nucl. Phys. **B643**, 431 (2002).
[74] M. Beneke and T. Feldmann, Nucl. Phys. **B592**, 3 (2001).
[75] M. Beneke and T. Feldmann, Nucl. Phys. **B685**, 249 (2004).
[76] M. Beneke and D. Yang, Nucl. Phys. **B736**, 34 (2006).
[77] G. Burdman and G. Hiller, Phys. Rev. D **63**, 113008 (2001).
[78] P. Ball and R. Zwicky, Phys. Rev. D **71**, 014029 (2005).
[79] A. Khodjamirian, T. Mannel, A. A. Pivovarov, and Y.-M. Wang, J. High Energy Phys. 09 (2010) 089.
[80] M. A. Ivanov, J. G. Korner, S. G. Kovalenko, and C. D. Roberts, Phys. Rev. D **76**, 034018 (2007).
[81] P. Ball and V. M. Braun, Phys. Rev. D **58**, 094016 (1998).
[82] P. Ball, V. M. Braun, Y. Koike, and K. Tanaka, Nucl. Phys. **B529**, 323 (1998).
[83] B. Grinstein, Y. Grossman, Z. Ligeti, and D. Pirjol, Phys. Rev. D **71**, 011504 (2005).
[84] A. Khodjamirian, T. Mannel, and Y. M. Wang, J. High Energy Phys. 02 (2013) 010.
[85] M. Dimou, J. Lyon, and R. Zwicky, Phys. Rev. D **87**, 074008 (2013).
[86] A. Hocker, H. Lacker, S. Laplace, and F. L. Diberder, Eur. Phys. J. C **21**, 225 (2001).
[87] C. Bobeth, M. Misiak, and J. Urban, Nucl. Phys. **B574**, 291 (2000).
[88] K. A. Olive (Particle Data Group Collaboration), Chin. Phys. C **38**, 090001 (2014).
[89] J. Charles, A. Höcker, H. Lacker, S. Laplace, F. R. Diberder, J. Malclés, J. Ocariz, M. Pivk, and L. Roos (CKMfitter Group Collaboration), Eur. Phys. J. C **41**, 1 (2005); updated results and plots available at http://ckmfitter.in2p3.fr.
[90] S. Aoki, Y. Aoki, C. Bernard, T. Blum, G. Colangelo, M. D. Morte, S. Drr, A. X. E. Khadra *et al.*, Eur. Phys. J. C **74**, 2890 (2014).
[91] R. Aaij *et al.* (LHCb Collaboration), J. High Energy Phys. 04 (2015) 064.
[92] C. Hambrock, G. Hiller, S. Schacht, and R. Zwicky, Phys. Rev. D **89**, 074014 (2014).
[93] D. Atwood, M. Gronau, and A. Soni, Phys. Rev. Lett. **79**, 185 (1997).
[94] M. Gronau, Y. Grossman, D. Pirjol, and A. Ryd, Phys. Rev. Lett. **88**, 051802 (2002).
[95] M. Gronau and D. Pirjol, Phys. Rev. D **66**, 054008 (2002).
[96] P. Ball and R. Zwicky, Phys. Lett. B **642**, 478 (2006).
[97] P. Ball, G. W. Jones, and R. Zwicky, Phys. Rev. D **75**, 054004 (2007).
[98] E. Kou, A. L. Yaouanc, and A. Tayduganov, Phys. Rev. D **83**, 094007 (2011).
[99] D. Becirevic, E. Kou, A. L. Yaouanc, and A. Tayduganov, J. High Energy Phys. 08 (2012) 090.
[100] B. Aubert *et al.* (*BABAR* Collaboration), Phys. Rev. D **72**, 051103 (2005).
[101] Y. Ushiroda *et al.* (Belle Collaboration), Phys. Rev. D **74**, 111104 (2006).
[102] Y. Amhis *et al.* (Heavy Flavor Averaging Group Collaboration), arXiv:1207.1158.
[103] G. Hiller and F. Kruger, Phys. Rev. D **69**, 074020 (2004).
[104] B. Gripaios, M. Nardecchia, and S. A. Renner, J. High Energy Phys. 05 (2015) 006.
[105] L. Hofer and J. Matias, J. High Energy Phys. 09 (2015) 104.
[106] S. Descotes-Genon and J. Virto, J. High Energy Phys. 04 (2015) 045.
[107] N. Haba, H. Ishida, T. Nakaya, Y. Shimizu, and R. Takahashi, J. High Energy Phys. 03 (2015) 160.
[108] A. Bharucha, D. M. Straub, and R. Zwicky, arXiv:1503.05534.